

SIGNAL TRANSDUCTION

A synthetic biology approach reveals diverse and dynamic CDK response profiles via multisite phosphorylation of NLS-NES modules

Ilona Faustova, Mihkel Örd, Viacheslav Kiselev, Dmytro Fedorenko, Irina Borovko, Dags Macs, Kaur Pääbo, Marko Lööke, Mart Loog*

The complexity of multisite phosphorylation mechanisms in regulating nuclear localization signals (NLSs) and nuclear export signals (NESs) is not understood, and its potential has not been used in synthetic biology. The nucleocytoplasmic shuttling of many proteins is regulated by cyclin-dependent kinases (CDKs) that rely on multisite phosphorylation patterns and short linear motifs (SLiMs) to dynamically control proteins in the cell cycle. We studied the role of motif patterns in nucleocytoplasmic shuttling using sensors based on the CDK targets Dna2, Psy4, and Mcm2/3 of *Saccharomyces cerevisiae*. We designed multisite phosphorylation modules by rearranging phosphorylation sites, cyclin-specific SLiMs, phospho-priming, phosphatase specificity, and NLS/NES phospho-regulation and obtained very different substrate localization dynamics. These included ultrasensitive responses with and without a delay, graded responses, and different homeostatic plateaus. Thus, CDK can do much more than trigger sequential switches during the cell cycle as it can drive complex patterns of protein localization and activity by using multisite phosphorylation networks.

INTRODUCTION

During major cellular reorganization events and state changes, such as cell division or cell differentiation, complex regulatory mechanisms and large spatially coordinated signaling networks are needed. In the eukaryotic cell division cycle, cyclin-dependent kinases (CDKs) are central regulators. In freely proliferating cells, CDK activity displays oscillatory dynamics due to the wavelike synthesis and degradation of cyclins (1). At each cell cycle stage, different versions of cyclins are expressed. In G_1 , the total CDK activity reaches a minimum due to the very low expression of cyclins and the low intrinsic activity of early CDK complexes (2–4). CDK activity starts to increase at the G_1/S transition, peaks in mitosis, and drops again at the M/G_1 transition (5).

The cell cycle is regulated by hundreds of CDK targets, leading to chains of downstream events, which are triggered by the phosphates added to target proteins [in *Saccharomyces cerevisiae*, there are ~700 CDK targets (6), which is >10% of the proteome]. However, it is not clear how the simple oscillatory dynamics of a single protein kinase activity can be processed into properly timed, dosed, and precisely localized molecular events that lead to synthesis, segregation, and division. One way CDK regulates protein activity is through the phospho-regulation of protein shuttling between the nucleus and cytoplasm (7, 8). However, little is known about how CDK can temporally control the ratio of nuclear and cytoplasmic concentrations in a precise manner to produce distinct protein activity dynamics.

Nucleocytoplasmic shuttling is mediated by the nuclear pore complex and karyopherins—importins and exportins that catalyze transport into the nucleus and cytoplasm, respectively. To be recognized, a target protein must carry a nuclear localization signal (NLS) and/or nuclear export signal (NES), which are amino acid sequences that are often regulated by multiple adjacent phosphorylation sites (9). Most CDK targets are phosphorylated at multiple sites (10). Multisite phosphorylation systems have been shown to introduce

ultrasensitivity to kinase output switches (11, 12), create multistability (13–15), facilitate multi-input signal processing (16–19) and allosteric regulation (20), regulate kinase scaffolds (21, 22), produce negative feedback (23), and form phospho-degrons (24, 25).

Our recent studies exemplified the power of the synthetic biology concept “build to understand” by demonstrating how multisite phosphorylation networks can act as “timing tags” that trigger specific events at distinct CDK thresholds. Using a model system based on the Cdk1 target Sic1, we changed the order of the sequence elements within phosphorylation site clusters to program the execution times over the whole time span of the budding yeast cell cycle (26, 27). The mechanisms that drive multisite phosphorylation by CDK include short linear motif (SLiM)-based cyclin docking interactions, priming phosphorylation, and docking of primed sites to the CDK complex’s phospho-adaptor subunit Cks1. The better the phosphorylation parameter set (or the “multisite phosphorylation code”) of a phosphorylation cluster is, the more efficiently CDK phosphorylates it up to the execution threshold of a switch. Thus, CDK function was translated into a simple principle as follows: Lower CDK activity at early cell cycle stages necessitates a stronger set of parameters in early targets, while the mitotic switches at higher CDK levels can contain sites or clusters with a relatively weak set of CDK multisite phosphorylation parameters. In this sense, a target can be compared to a resistor in electronics. The higher the resistance is, the later the switch. By counteracting CDK activity, phosphatases play a key role in determining the CDK activity threshold of a switch. For example, a preference for phospho-threonine dephosphorylation over phospho-serine by PP2A-Cdc55 creates a delay in threonine phosphorylation in the cell cycle (28).

In these previous studies, we focused solely on how the multisite phosphorylation parameters that lead to faster or slower phosphorylation can control a fixed output condition, i.e., the generation of a phospho-degron (26, 27). However, there are many types of CDK signaling outputs (7), which can be regulated in multiple ways, including the following: complex formation/disruption, localization

Copyright © 2022
The Authors, some
rights reserved;
exclusive licensee
American Association
for the Advancement
of Science. No claim to
original U.S. Government
Works. Distributed
under a Creative
Commons Attribution
NonCommercial
License 4.0 (CC BY-NC).

Institute of Technology, University of Tartu, Tartu 50411, Estonia.

*Corresponding author. Email: mart.loog@ut.ee

change, enzyme activation/inactivation, protein degradation, etc. Moreover, the same type of outputs may have different affinities or execution rates for the subsequent downstream processes. Thus, it remains an open question whether phosphorylation efficiency is a generalizable predictor of output timing, i.e., poor CDK sites (or sites with a low CDK/phosphatase specificity ratio) are later switches, while optimal CDK sites or docking-potentiating sites are early switches. One mechanism that can subvert this direct relationship is cyclin-specific docking (18, 27, 29–34). Cyclin-specific docking can enforce a well-resolved temporal order of substrate phosphorylation that is independent of the phosphorylation site specificity (26). This was also elegantly demonstrated in a recent study comparing the phosphorylation dynamics of Cdk1 substrates in wild-type (WT) strains to a strain with just one B-type cyclin, Clb2, instead of six (Clb1 to Clb6) (10). Similarly, the relationship between phosphorylation efficiency and output timing can also become confounded when the rates of downstream steps are taken into account. For example, substrates with the same timing for CDK phosphorylation can have different timing for the resulting output effects, such as nuclear exit, due to differences in the kinetics of downstream steps (fig. S1A).

In the current paper, we addressed the relationship between phosphorylation efficiency and response dynamics focusing on multisite phosphorylation of NLS-NES modules. In contrast to degradation, phospho-regulation of localization is a more complex reversible output, opening up a much richer set of possibilities in terms of the response profiles. We used synthetic phospho-regulated nuclear localization sensors based on NLS-NES regions of the CDK targets Dna2, Psy4, and Mcm2/3 in *S. cerevisiae*. Instead of a fixed CDK output, the studied phosphorylation sites and their CDK specificity affected both the net rate of CDK multisite phosphorylation of the sensor and the dynamics of the downstream process, namely, nucleocytoplasmic shuttling, via differential regulation of the NLS and NES. By varying the combination of phosphorylation sites and by introducing different cyclin-specific docking motifs, we found that the dynamic output profiles of nuclear entry or exit, as a response to accumulating cyclins from G₁ to mitotic exit, can exhibit very different shapes and oscillatory behaviors.

RESULTS

Switching between abrupt and gradual nuclear exit profiles of a Psy4-based CDK sensor

To create a localization sensor that exits the nucleus in response to CDK activity, we fused superfolder green fluorescent protein (sfGFP) to the intrinsically disordered C terminus of Psy4 (positions 315 to 441) (Fig. 1A and fig. S1B), a regulatory subunit of the protein phosphatase PP4 that contains a bipartite NLS, which is inactivated by Cdk1-mediated phosphorylation (8, 35). We followed the nuclear shuttling of the construct using time-lapse fluorescence microscopy (Fig. 1B). We used the G₁/S transition, defined as a point at which 50% of an Mcm2/3-based Cdk1 activity sensor tagged with mCherry was exported from the nucleus, as a reference point of cell cycle progression (Fig. 1C and fig. S1C) (18, 36). In addition, we used the Mcm2/3-based sensor to measure the cell cycle length and found that, in these experiments, 25% of cells reach anaphase by 54 min after G₁/S transition (Fig. 1C). Psy4(full-length)-sfGFP (78 kDa) and Psy4(315–441)-sfGFP (42 kDa) were exported from the nucleus with similar dynamics following G₁/S (Fig. 1C). This confirms that the disordered C terminus could be used as a model system to study the

regulation of nuclear shuttling and that the localization dynamics were not affected by a possible gain in free diffusion through the nuclear pores for the smaller protein. Additionally, the addition of glutathione S-transferase to Psy4(315–441)-sfGFP, which increased the molecular weight by 27 kDa, did not affect the localization dynamics, indicating that the process is dependent on regulated transport (Fig. 1C).

Double mutation of the optimal CDK phosphorylation sites T320 and T347 to alanines leads to constant nuclear localization of Psy4 during the cell cycle (Fig. 1, A and D) (8). These sites are located immediately N-terminal to the two basic motifs of the bipartite NLS (Fig. 1A), and their phosphorylation is expected to inhibit nuclear import (Fig. 1E) (8). However, the disordered C terminus contains four additional Cdk1 consensus sites (Fig. 1A). To study the potential complexity of the six-site network in regulating nucleocytoplasmic shuttling, we performed systematic analysis using phosphorylation site mutants. First, we found that the single alanine mutation T347A did not abolish exit in contrast to the double mutant but instead switched the rapid drop of nuclear signal to a slow gradual decline (Fig. 1D). The T320A mutant also exhibited a less steep decline, although the effect was less drastic (Fig. 1D), but we observed no effect upon mutation of a minimal consensus site S337 (fig. S1D).

As the exit of the T347A mutant is not abrupt, the phosphorylation-driven switch cannot be attributed to a specific CDK activity threshold. In contrast, the WT sensor exhibits an abrupt switch-like exit. This raises the possibility that different dynamic shapes of CDK signaling outputs can be created via the phosphorylation of multisite networks that regulate the equilibrium of nucleocytoplasmic shuttling. As T347 is a site at which phosphorylation is predicted to hinder nuclear import, the gradual decline instead of a rapid switch is likely due to the increased re-entry rate of the T347A sensor (fig. S1E). Thus, for the WT sensor, the downstream event at the G₁/S threshold (translocation into the cytoplasm) is very efficient. The localization equilibrium is abruptly shifted toward exit at very low CDK activity levels via CDK-blocked re-entry. However, when re-entry is blocked less efficiently, due to the T347A mutation, the abrupt exit is switched to a gradual decline. These results exemplify how a single CDK site mutation in a six-site phosphorylation network can switch the kinase-phosphatase module input-output function from the one with an ultrasensitive response to a graded response (12). The WT sensor showed cell cycle-dependent phosphorylation shifts, with the major change starting at 20 to 30 min after release from G₁ (Fig. 1F), which correlates well with the microscopy profile of a fast drop in nuclear localization (Fig. 1C). The version with T347A showed a slower accumulation of the shifts, which was also in good agreement with the slow gradual exit observed by microscopy (Fig. 1, D and F).

The abrupt trapping of the phosphorylated sensor in the cytoplasm as opposed to the leaking circulation would suggest that engineering a more efficient and specific phosphorylation of the NLS-inactivating sites at the leaking sensor would restore the ultrasensitive response. To test this hypothesis, we engineered sensors with increased cyclin recognition specificity. The WT Psy4(315–441) fragment lacks any identified cyclin docking motifs, and the addition of an optimal G₁-CDK-specific LP cyclin docking motif (32) did not substantially change its rapid exit (Fig. 1G and fig. S1E). In contrast, adding this LP motif to the T347A mutant transformed its gradual exit profile to an early abrupt ultrasensitive switch and shifted the 50% exit timing by approximately 40 min (Fig. 1G). This result suggests that the CDK thresholds and temporal order of switches based on different multisite phosphorylation patterns

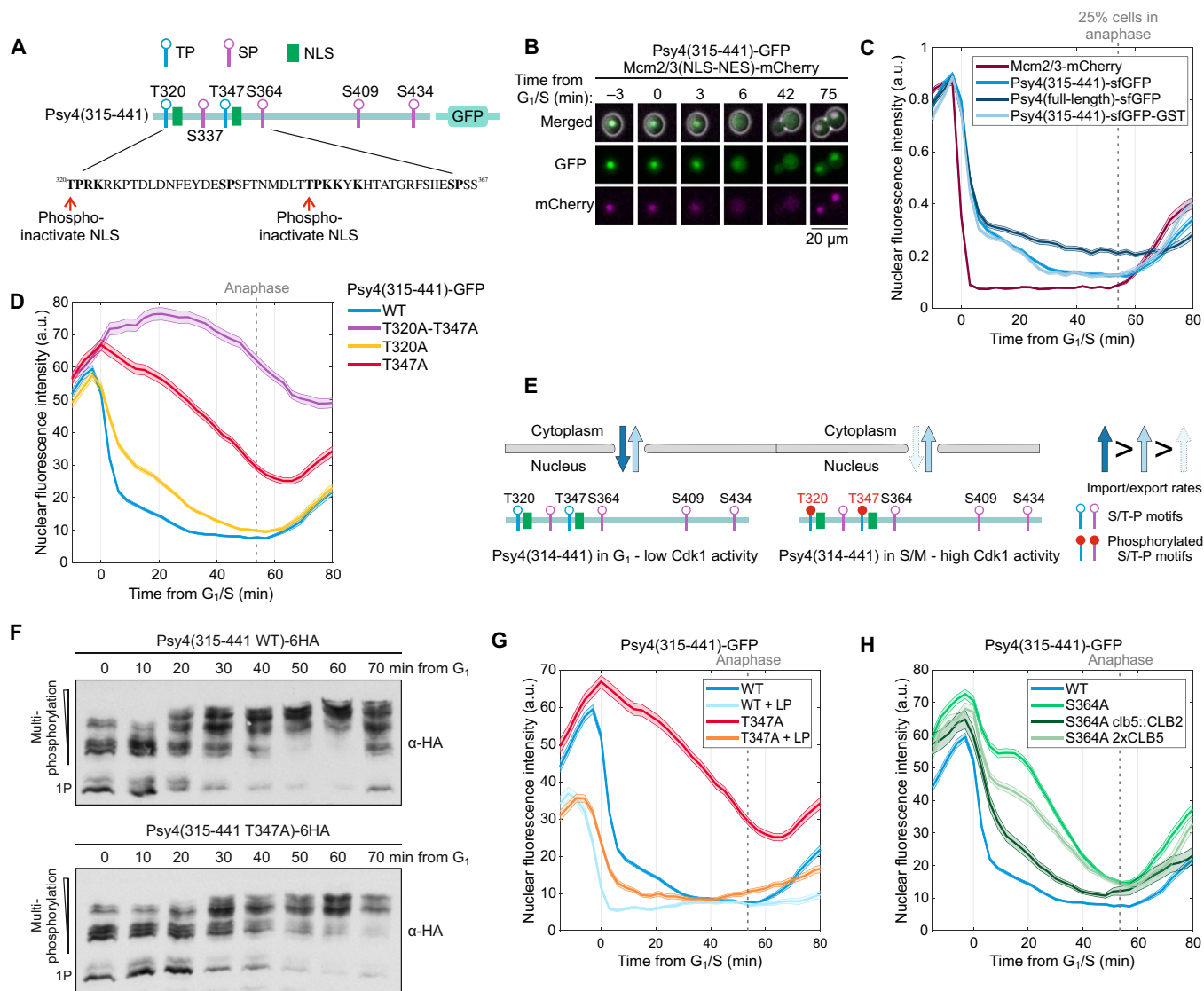


Fig. 1. Multisite phosphorylation controls the nuclear export of Psy4. (A) Scheme showing the Cdk1 phosphorylation sites and NLS motifs in the disordered C terminus of Psy4 (positions 315 to 441). Phosphorylation of T320 and T347 inactivates the NLS (8). (B) Images showing the cell cycle–dependent shuttling of Psy4(315–441)-GFP and Mcm2/3(NLS–NES)-mCherry sensor between the nucleus and cytoplasm. (C) Normalized nuclear fluorescence intensities of the indicated Psy4 modules during the cell cycle. Plot shows means \pm SEM of cells synchronized at the time of G₁/S, defined by nuclear export of 50% of the Mcm2/3 NLS–NES sensor. GST, glutathione S-transferase. (D) Plot displaying means \pm SEM nuclear fluorescence intensities of a population of cells expressing different Psy4-based modules synchronized at G₁/S by the Mcm2/3 sensor. (E) Scheme illustrating the nuclear import/export kinetics of the Psy4 sensor without phosphorylation in G₁ or upon phosphorylation in S and M phases. (F) Phosphorylation of the Psy4 modules was studied in cell cultures synchronized in G₁ with α -factor and released to the cell cycle. Different phospho-forms were separated using Phos-tag SDS–polyacrylamide gel electrophoresis (PAGE). (G) Plot showing the means \pm SEM nuclear fluorescence levels of the Psy4 sensors in the cell cycle. The LP motif (VLLPPFRI) was added to the C terminus of Psy4, as shown in fig. S1E. (H) Nuclear export of Psy4-S364A module in different strains. In *clb5::CLB2* strain, an extra copy of *CLB2* is expressed from *CLB5* locus, and in *2xCLB5* strain, an extra copy of *CLB5* is expressed from an integrative plasmid. Plot shows means \pm SEM nuclear Psy4-GFP fluorescence intensities. a.u., arbitrary units.

depend heavily on the kinetics of both phosphorylation and post-phosphorylation downstream equilibria (also see fig. S1A).

Cyclin specificity imposes a biphasic nuclear exit profile for the sensor in S and M phases

Unexpectedly, a single alanine mutation at S364 caused a stepwise biphasic nuclear drop of the sensor (Fig. 1H and fig. S1E). An initial rapid export after G₁/S was followed by a period of steady plateau around the S phase of up to 20 min, after which the exit rate increased

again. Apparently, as also demonstrated in more detail below, the kinase-phosphatase specificities toward the key sites in the S364A sensor enable rapid phosphorylation and rapid steady-state equilibrium (plateau) upon reaching the S-CDK peak, while the phosphorylation of key sites in the T347A sensor must be slower; thus, equilibrium cannot be reached before the later mitotic cyclins start to accumulate. As S364 does not qualify as a predicted site affecting the NLS (8), the incomplete exit in S phase suggests that S364 could be a positive regulator of a putative NES.

To test whether it is possible to shift the S phase equilibrium and the plateau height by increasing CDK activity in S phase, we used a well-defined system in which the S phase cyclin *CLB5* was replaced in its locus with mitotic cyclin *CLB2* (37). As the intrinsic catalytic activities of CDK complexes rise gradually during the cell cycle (2, 3, 34), Clb5-Cdk1 has approximately an order of magnitude lower specificity toward CDK consensus phosphorylation sites compared to that of Clb2-Cdk1. As expected, the *clb5::CLB2* replacement [in the $\Delta swe1$ background (37, 38)] suppressed the plateau and almost restored the dynamics of the WT sensor (Fig. 1H). Similarly, when a second copy of *CLB5* was added, the plateau was shifted, although not as much as in the case of Clb2 (Fig. 1H),

which is also in agreement with in vitro kinetic data on the intrinsic activity differences of these two CDK complexes (34). Thus, the biphasic dynamics corresponded to profound differences in S- and M-CDK intrinsic activities. Intriguingly, the observed profile is an example of how CDK-regulated processes in two major phases of the cell cycle, S and M phases, could clearly manifest as two different output steady states.

A mitotic switch based on limited phospho-regulation of NLS and NES

Notably, the S phase plateau of the S364A mutant shifted up when the T320A mutation was added (Fig. 2A), creating a profile with

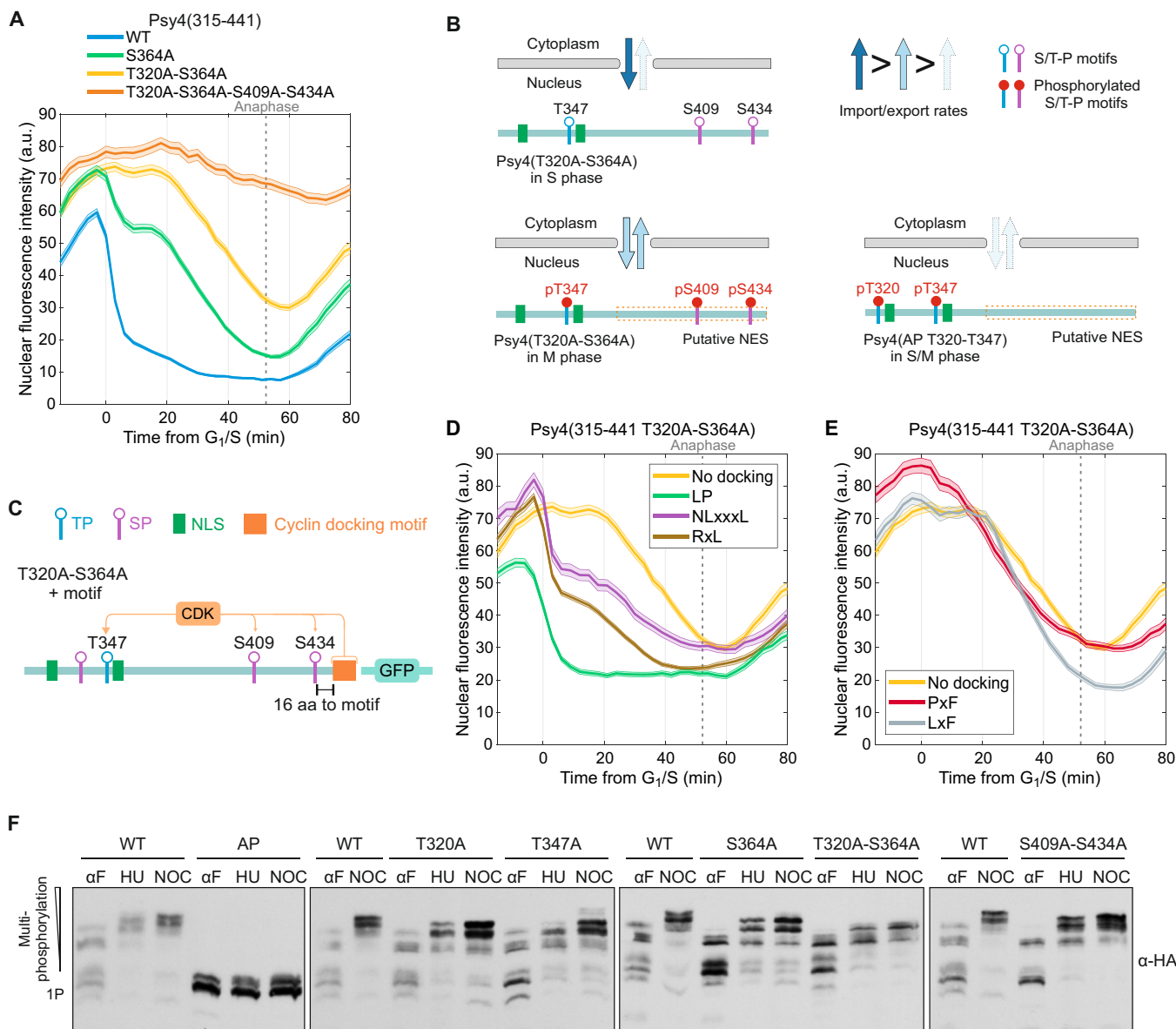


Fig. 2. Combined mutations generate a mitotic localization switch. (A) The nuclear fluorescence of the indicated Psy4 modules with different phosphorylation site mutations was studied in time-lapse microscopy. Plot shows the means \pm SEM Psy4-GFP nuclear fluorescence intensity. (B) Schemes illustrating the relative nuclear import/export kinetics estimated from the microscopy experiments for the indicated Psy4(315-441)-GFP sensors presented in (A) and fig. S2A. (C) Scheme showing the positioning of phosphorylation sites and added cyclin docking motifs in the Psy4 module. aa, amino acids. (D and E) Effect of cyclin docking motif addition to T320A-S364A Psy4 module. Plots show means \pm SEM of the Psy4-GFP nuclear level from cells synchronized at G₁/S during analysis. (F) Cells were arrested either in G₁ with α -factor (α F), in S phase with hydroxyurea (HU), or in mitosis with nocodazole (NOC). The multisite phosphorylation of the indicated Psy4 module was studied using Phos-tag SDS-PAGE Western blotting. AP denotes Psy4 mutant, where all CDK consensus phosphorylation sites are mutated to alanines.

virtually no response to premitotic thresholds of CDK activity. When the most C-terminal sites of the six-site cluster, the suboptimal SP motifs S409 and S434, were further mutated, the construct became entirely nuclear. As these sites are located at least 40 amino acids C-terminal to the NLS, their phosphorylation is not expected to affect the NLS (8). This suggests that, similar to S364, phosphorylation of these sites might activate a putative NES (Fig. 2B). Psy4 is exported by Msn5, for which no NES consensus has been defined, but the export of other Msn5 targets has been found to be activated by phosphorylation (8, 39). Thus, the data suggested that, in the T320A-S364A construct, the two mutations weakened both NLS and NES regulation. Low levels of CDK in S phase are not sufficient to shift the equilibrium toward exit, while the higher mitotic levels are still sufficient to achieve this shift (Fig. 2B). To test this hypothesis, we attempted to increase the S-CDK activity toward the T320A-S364A sensor by introducing cyclin-specific docking motifs (Fig. 2C). The addition of an optimal G₁-specific LP motif resulted in rapid export of the sensor at G₁/S (Fig. 2D). An exclusively S-Cdk1-specific NLxxxL motif (27) led to an abrupt partial exit, followed by a gradual decline in nuclear levels (Fig. 2D), while the addition of an RxL motif resulted in a slightly steeper decline after the initial drop, which is in good agreement with the high specificity of RxL motifs for S-Cdk1 and moderate specificity for the G₂-Cdk1 complex (33). The M-Cdk1-specific LxF motifs exhibited a mild effect on the slope of the exit around the time window of mitosis (Fig. 2E). Similarly, the profile created by addition of the G₂-Cdk1-specific PxF motif correlates with the expression period of G₂ cyclin Clb3 between S and M phase cyclins.

In addition, a sensor containing the pair T320 and T347 as the only two CDK sites left (AP T320-T347, where AP denotes the mutation of all CDK consensus sites except for those noted) was able to shift the equilibrium between the nucleus and cytoplasm (Fig. 2B and fig. S2A). This suggests that basal NES activity must be present in a nonphosphorylated construct, as active export by Msn5 is necessary for the nuclear exit of Psy4, and phosphorylation of T320 and T347 is predicted to affect NLS re-entry but not the exit rate (Fig. 2B) (8). Furthermore, when either T320 or T347 was present as the single CDK consensus site, the construct was entirely nuclear (fig. S2A). This suggests that pT320 and pT347 work as a cooperative pair to prevent re-entry.

C-terminal truncations in Psy4 suggested that an NES could reside in the region around the CDK site S364 and the region from 375 to 441 that harbors the CDK sites S409 and S434 (fig. S2, B and C). To further test the export activity of this region, we replaced the identified Crm1-dependent NES in the Mcm2/3 NLS-NES sensor with the Psy4 sequence from positions 360 to 441 (fig. S2D). While mutating the Mcm3 NES led to a considerable loss in nuclear shuttling of the sensor, replacing the Mcm3 NES with the Psy4(360-441) region rescued the shuttling; however, compared to the construct with the Mcm3 NES, this construct remained more nuclear (fig. S2E). Mutation of Psy4 S364, S409, and S434 to alanine abolished the nuclear export activity of this region when fused to the Mcm2/3 NLS (fig. S2E). This finding indicates that the Psy4 region at positions 360 to 441 has phosphorylation-dependent nuclear export activity. In the Psy4(315-441) construct, a double mutation of S409A-S434A in the WT template did not affect the localization, but reduced nuclear export upon S409A and S434A mutations was observed when combined with that of the T347A mutation (fig. S2F). Therefore, in contrast with the S364A mutant (Fig. 2A), we suggest that phosphorylation of S364 is the major determinant of export promoting activity, while sites S409 and S434 may have a supportive role.

Next, we directly analyzed the phosphorylation of the localization modules in different cell cycle phases. For this, we arrested cells with α -factor (G₁ phase), hydroxyurea (HU) (S phase), or nocodazole (mitosis) (Fig. 2F). Separate mutations of T320A, T347A, or S364A showed a single-band downshift of the hyperphosphorylation in nocodazole. In addition, the double mutation T320A-S364A caused a further loss of phosphorylation in HU, while a slightly prominent shift in mitosis was observed (Fig. 2F). The double mutation S409A-S434A showed a moderate loss in phosphorylated forms in HU and nocodazole arrest, which confirms that these sites are phosphorylated *in vivo* and may play a role in promoting nuclear exit, as observed in several forms of the sensor (Fig. 2A and fig. S2F).

NLS-regulating phosphorylation sites are linked to NES-activating sites via Cks1-mediated docking

Kinase assays using purified proteins and Phos-tag SDS-polyacrylamide gel electrophoresis (PAGE) autoradiography revealed that phosphorylation of the WT sensor is dependent on Cks1, a phospho-adaptor subunit of the CDK complex that recognizes phospho-threonines but not phospho-serines as priming sites (Fig. 3A) (40, 41). Cks1-dependent docking facilitates the phosphorylation of sites located on the C-terminal side of the priming sites (41). For example, the NLS-inactivating TP sites could prime the C-terminal export-activating SP sites (Fig. 1A). This directional chain of priming events that leads to the phosphorylation of SCF phospho-degrons has been found in several CDK targets (18, 25, 27). Phosphorylation of constructs containing T320A or T347A mutations, alone or combined, revealed that T320 and T347 are the major Cdk1 target sites and are required for rapid Cks1-dependent hyperphosphorylation (Fig. 3B).

To further test whether T320 or T347 may be the priming sites facilitating the phosphorylation of export-activating sites, we used phospho-mimetic mutations T320E and T347E and followed their localization dynamics. The idea was to separate the two functions: While the glutamates may mimic the phospho-regulation of NLS, as reported (36), they cannot act as priming sites since the phospho-mimicking EP sequences do not bind Cks1 (40). As expected, both T320E and T347E reduced the initial nuclear localization level of the construct, confirming that these mutations inactivate the NLS (Fig. 3C). On the other hand, after G₁/S, the T320E mutant followed the same exit profile as that of the WT sensor, whereas the T347E mutant showed a gradual exit path, analogous to the T347A mutant (Figs. 1D and 3C). This result strongly suggests that phosphorylated T347 (pT347) serves as a Cks1-dependent priming site to promote the phosphorylation of the NES-activating site S364 (Fig. 3D). Although pT320 might also act as a primer for S364, the distance between the two sites exceeds the optimum length (41), which may also be reflected in the slow gradual exit of the T347A sensor (Fig. 1D). In addition, the synergistic amplification from Cks1 docking is clearly evident from the finding that sensors including either the Cks1 primer site (T347) or the suboptimal sites (S364, S409, and S434) are entirely nuclear, but combining them into one sensor creates a prominent early switch (fig. S3A).

This intriguing priming-mediated connection between NLS-inactivating and NES-activating sites further reveals that the whole six-site CDK phosphorylation network contains a more complex signal processing scheme than that initially anticipated. The priming connection may work as a system to ensure that molecules containing the NLS-inactivating pT347 site are exported decisively. In the absence of this connection, randomly distributed phosphorylation of

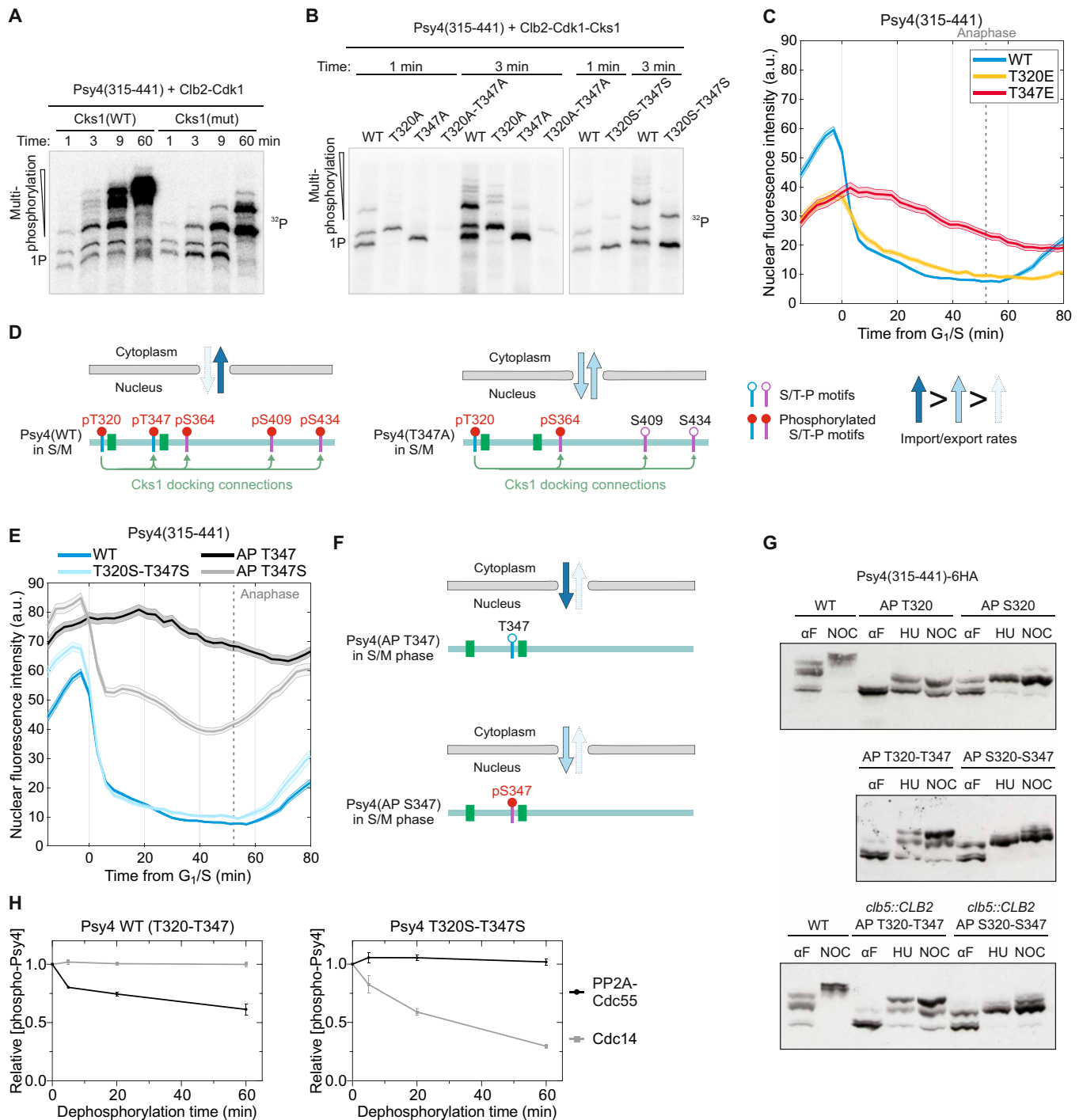


Fig. 3. Multiple effects of Thr-to-Ser mutations in positions 320 and 347. (A) The multisite phosphorylation of Psy4(315-441)-GFP by Clb2-Cdk1 in complex with either WT or mutated Cks1 was studied in vitro using Phos-tag SDS-PAGE ³²P autoradiography. (B) In vitro analysis of site specificity and the contribution of Cks1 primer sites on Psy4 multisite phosphorylation by Clb2-Cdk1. The proteins were resolved on Phos-tag SDS-PAGE ³²P autoradiographs are shown. (C) The effect of phospho-mimicking mutations in positions 320 and 347 was studied in microscopy; plot displays means ± SEM of nuclear fluorescence intensities of the indicated Psy4-GFP module. (D) Schemes illustrating the effect of T347A mutation on the nuclear import/export kinetics and Cks1 docking connections in Psy4(315-441)-GFP. (E) Effect of T/S mutations on the nuclear levels of Psy4(315-441)-GFP. Plot shows means ± SEM nuclear intensities of cells aligned at the time of G₁/S. (F) Depiction of estimated relative nuclear shuttling kinetics of Psy4(315-441)-GFP with T347 or S347 as the only CDK phosphorylation site. (G) Phosphorylation pattern of Psy4 modules in synchronized cell cultures was studied using Phos-tag SDS-PAGE Western blotting. (H) The effect of Thr-to-Ser mutations on the dephosphorylation rate of the Psy4 module was studied in vitro using PP2A-Cdc55 and Cdc14 to dephosphorylate Psy4(315-441)-GFP prephosphorylated by Clb5-Cdk1. Plot shows means ± SD of the relative remaining phospho-³²P Psy4 signal at indicated time points.

T347 or S364 sites in a pool of molecules may either not lead to efficient export or may result in a futile export-import cycle, respectively (Fig. 3D).

Threonine-serine swapping reveals a CDK specificity filter

As Cks1 binds phospho-threonines but not phospho-serines, we tested a Cks1-docking deficient T320S-T347S mutant sensor. This sensor was exported rapidly at G₁/S, similar to the WT (Fig. 3E). There are two possible explanations for this result, including the following: either the Cks1-dependent docking is not important or the phosphorylation of serines at sites 320 and 347 occurs more efficiently than that of threonines and thereby rescue the effect of disabled Cks1 docking. A construct with T347 as the only CDK site was almost stable over the cell cycle, but a similar construct with the T347S mutation resulted in rapid exit, dropping to 50% of G₁ levels (Fig. 3E). In constructs with T320 or S320 as the only CDK sites (AP T320 or AP T320S), the effect was similar (fig. S3B). These results support the possibility that phosphorylation at sites 320 and 347 occurs to a greater extent (i.e., a greater fraction of molecules) when they are serines than when they are threonines (Fig. 3F). In addition, other sensor versions with threonine-serine mutations showed a switch to a similar rapid loss of nuclear localization at G₁/S (fig. S3, C to E).

Next, we compared the dynamics of Psy4 modules with T320-T347 and S320-S347 as the only two CDK sites in a strain in which the *CLB5* gene was replaced with *CLB2* (*clb5::CLB2 Δswe1*) to obtain higher intrinsic Cdk1 activity in S phase, as described above (Fig. 1H). While the AP T320S-T347S sensor oscillated with similar dynamics in the WT and *clb5::CLB2* strains, the AP T320-T347 module was exported to a greater extent in the *clb5::CLB2* strain (fig. S3F). This suggests that S320 and S347 could be close to being maximally phosphorylated in the S phase, whereas T320 and T347 did not reach full phosphorylation in the WT background. To assess the phosphorylation status, we analyzed the shifts in cells arrested with α -factor (G₁), HU (S phase), or nocodazole (mitosis) using Phos-tag Western blotting. As predicted, the AP T320S-T347S sensor and AP S320 sensor reached a full shift compared to that of the analogous threonine variants (Fig. 3G). While the AP T320-T347 sensor was phosphorylated to a greater extent in HU-arrested *clb5::CLB2* cells than in WT cells, it did not reach full phosphorylation in the mitotic cells of either strain (Fig. 3G). This suggests that serines in these positions are efficiently and fully phosphorylated, but threonines are not.

We and others have previously shown using model substrate peptides that compared to TP motifs, SP motifs are approximately two to three times more specific for Cdk1 complexes (26, 42). In addition, with Psy4 sensors, we found that the T320S-T347S mutant showed a loss of hyperphosphorylation in vitro but also an increase in the phosphorylation initial velocity by two times (Fig. 3B). Next, we found that, in in vitro dephosphorylation assays, a key CDK counteracting phosphatase PP2A-Cdc55 showed a higher preference for the WT Psy4 sensor containing the two threonines compared to the T320S-T347S version (Fig. 3H and fig. S3G). This is in agreement with previous reports on PP2A-Cdc55 specificity, which also found that the serine-threonine identity of phosphorylation sites is a key determinant of the timing of site phosphorylation in the cell cycle (28, 43). Lower CDK specificity and higher phosphatase specificity could explain why export is less efficient with the sensors containing T320 and/or T347 compared to the corresponding sensors with Thr-to-Ser mutations. In contrast, the phosphatase Cdc14, which counteracts CDK during mitotic exit, showed a higher specificity

for the T320S-T347S sensor (Fig. 3H and fig. S3G), which is also in agreement with a previously reported preference for phosphoserines in the case of Cdc14 (44, 45). These data demonstrate that even highly optimal CDK sites can be only partially phosphorylated due to high phosphatase specificity.

As previously shown for several Cdk1 targets, S/TP consensus sites can be phosphorylated in G₁ when the activity of cell cycle-related CDK complexes is very low (17, 26), and we found that the Psy4-based sensor was partially phosphorylated in an α -factor arrest (Figs. 1F, 2F, and 3G). However, most of these shifts were not present when an alternative approach by G₁ cyclin depletion was used for G₁ arrest, suggesting that the phosphorylation was due to the mitogen-activated protein kinase Fus3 that is activated via the pheromone pathway (fig. S4A). Psy4 is nuclear in pheromone-induced G₁ arrest (8), raising the interesting possibility of a specificity filter that allows nuclear exit only in response to Cdk1, which, in contrast to other proline-directed kinases, has the Cks1 docking mechanism.

The T320S-T347S sensor lacks the Cks1 docking capability, while its phosphorylated form is more resistant to phosphatases (providing a lower phosphorylation threshold for proline-directed kinases compared to that of the threonine-based sites) (28). To test the effect of Thr-to-Ser mutations on filtering kinase activity, we analyzed the levels of the WT sensor and the T320S-T347S sensor in an α -factor arrest. The WT sensor accumulated to higher levels compared to that of the all-Ser version in G₁ (fig. S4, B and C). In addition, in an α -factor arrest, the sensor with all Cdk1 consensus sites mutated to alanine accumulated to higher nuclear concentrations compared to that of the T320A-T347A mutant, in which S364, S409, and S434 were still present (fig. S4, D and E). This further supports that the sites S364, S409, and S434 promote nuclear export and that these sites are phosphorylated to some extent in cells arrested with α -factor. These experiments show the importance of serine-threonine identity of phosphorylation sites in determining the phosphorylation threshold, which affects both the phosphorylation dynamics in the cell cycle and filtering the input from different kinases.

The Cdk1 inhibitor sensitivity of the G₁/S triggered sensors and the concept of CDK thresholds

To test how the localization sensors behaved in the context of different Cdk1 activity dynamics, we inserted them into the Cdk1-as1 strain (46), in which Cdk1 activity is lower and can be quantitatively inhibited. The Mcm2/3-based sensor was exported with similar fast kinetics at G₁/S as in a WT strain, and the profile was not sensitive to up to 200 nM inhibitor (Fig. 4A). Notably, in the case of the Psy4-based sensor, the profile was changed from an ultrasensitive G₁/S switch to a gradual export in the Cdk1-as1 strain. Furthermore, even a small 100 nM dose of inhibitor, which was insufficient to induce cell cycle arrest at a high G₂/M CDK threshold (46), led to a markedly flattened nuclear shuttling profile of the Psy4-based module with a minor nuclear exit in the cell cycle (Fig. 4B). A similar effect was observed with the S364A mutant sensor (Fig. 4C), whereas the inhibitor had no effect on the localization sensor dynamics in cells expressing WT Cdk1 (fig. S4F). This differential inhibitor sensitivity might arise from the serine-threonine preferences of both phosphatases and Cdk1, as the NLS-inactivating sites are serines in the Mcm2/3 sensor and threonines in the Psy4 sensor. The sensitivity to the inhibitor is highest when sites are not fully phosphorylated (Fig. 4, D and E). In addition, in multistep phosphorylation systems, the final inhibitor effect is amplified at each sequential step.

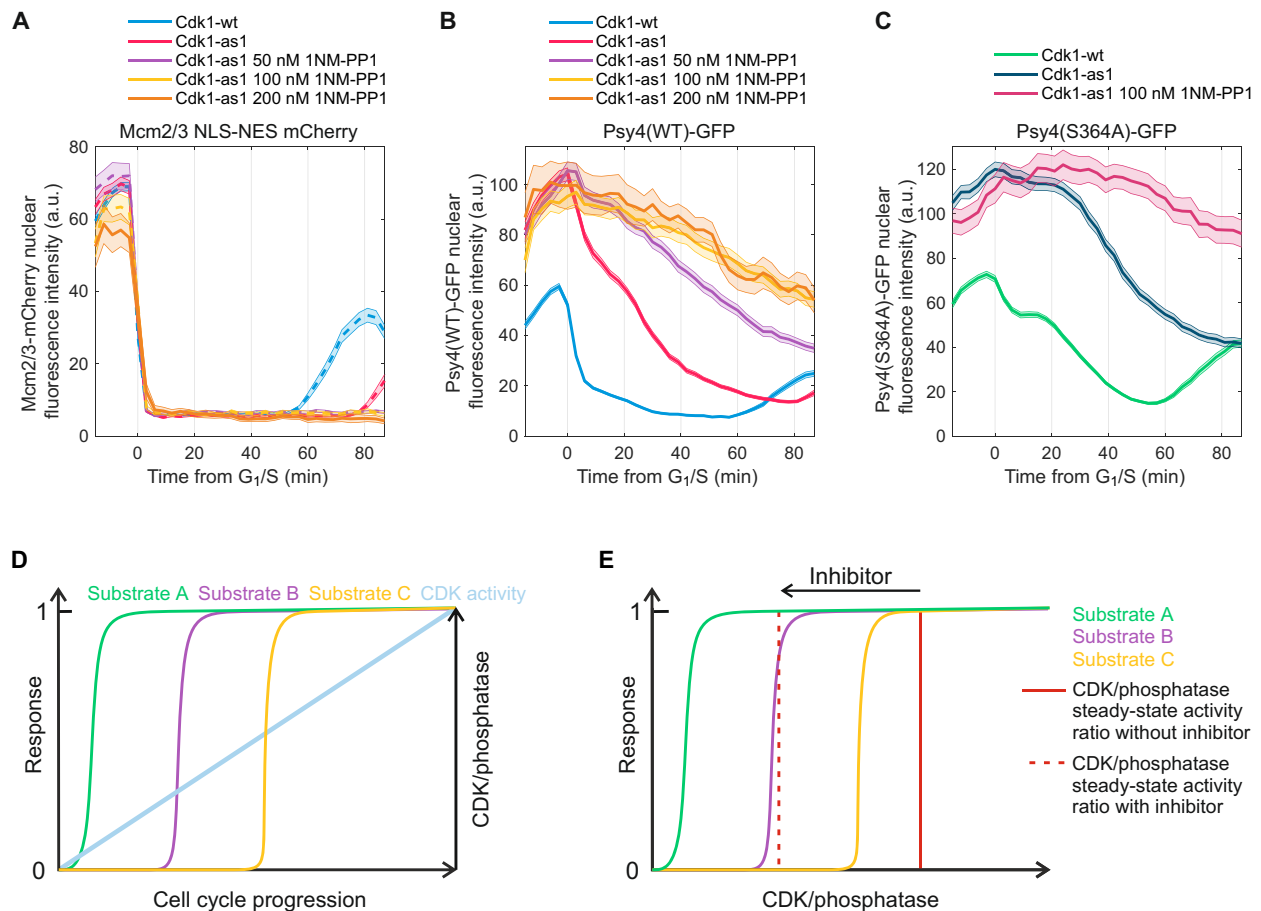


Fig. 4. Differential sensitivity of G₁/S targets to partial Cdk1 inhibition. (A to C) Localization dynamics of Psy4(315-441)-GFP and Mcm2/3(NLS-NES)-mCherry during the cell cycle in the presence of 1NM-PP1, the inhibitor of analog-sensitive Cdk1-as1. Plots show means \pm SEM nuclear fluorescence intensities of Mcm2/3(NLS-NES)-mCherry in (A), Psy4(315-441 WT)-GFP in (B), and Psy4(315-441 S364A) in (C). (D) Scheme showing an ultrasensitive response of substrates A, B, and C triggered at different ratios of kinase/phosphatase activities as the CDK activity increases. (E) Scheme illustrating the effect of partial kinase inhibition (by addition of 1NM-PP1) on the response triggered by phosphorylation of substrates A, B, and C. Addition of inhibitor decreases the ratio of kinase to phosphatase activities, leading to full inhibition of substrate C response, partial inhibition of substrate B response, and no effect to substrate A response.

Thus, the Psy4 sensor could be sensitive to lower doses of inhibitor because of the stepwise process involving Cks1 docking via pT347, which is crucial for the phosphorylation of the C-terminal sites. Nevertheless, these results are unexpected because they indicate that targets with similar phosphorylation timings (and presumably similar CDK thresholds) show very different sensitivities to Cdk1 inhibitors. These results introduce alternative possibilities to interpret the use of inhibitor doses to define CDK thresholds.

A nuclear import module based on Dna2 also depends on CDK multisite phosphorylation

To study an example of CDK-activated nuclear import, we engineered a minimal model system based on the DNA replication factor Dna2. The Dna2 protein contains an intrinsically disordered N terminus with a bipartite NLS that is activated by a Cdk1-mediated phosphorylation of S17 in the linker region of the NLS (Fig. 5A) (8). We fused the 100 N-terminal residues of Dna2 to sfGFP and expressed it from the constitutive *P_{ACT1}* promoter to study the regulation of Cdk1-controlled nuclear entry using time-lapse fluorescence microscopy (Fig. 5B). Dna2(1-100)-GFP was mainly cytoplasmic in

the G₁ phase but accumulated rapidly in the nucleus after G₁/S (Fig. 5, B and C). Mutation of Cdk1 site S17 abolished the nuclear entry of the module (Fig. 5C), as reported previously for full-length Dna2 (8). Full-length Dna2 showed similar localization dynamics as those of the N-terminal fragment (fig. S5A), indicating that the key motifs regulating the localization are in the 1-to-100 fragment.

Next, we tested how the CDK specificity of S17 affects the dynamics of nuclear entry. We generated two constructs in which the S17 motif (SPAKK) was mutated to a minimal consensus site (SPAQQ or SPAAK). These mutations caused an approximately 50% drop in the nuclear abundance during the cell cycle but did not have a notable effect on the timing of nuclear entry (Fig. 5D). Another full consensus CDK phosphorylation site, T4, is located 13 residues upstream of S17 at an ideal distance to act as a Cks1-dependent phospho-priming site for S17 (Fig. 5A). To test this idea, we mutated T4 either to alanine or serine. Both mutations caused a considerable decrease in nuclear accumulation of Dna2(1-100)-GFP and slightly delayed the timing of entry (Fig. 5E), suggesting that T4 functions as a Cks1-dependent primer site for the phosphorylation of S17. Furthermore, when the mutation of S17 to a minimal consensus site

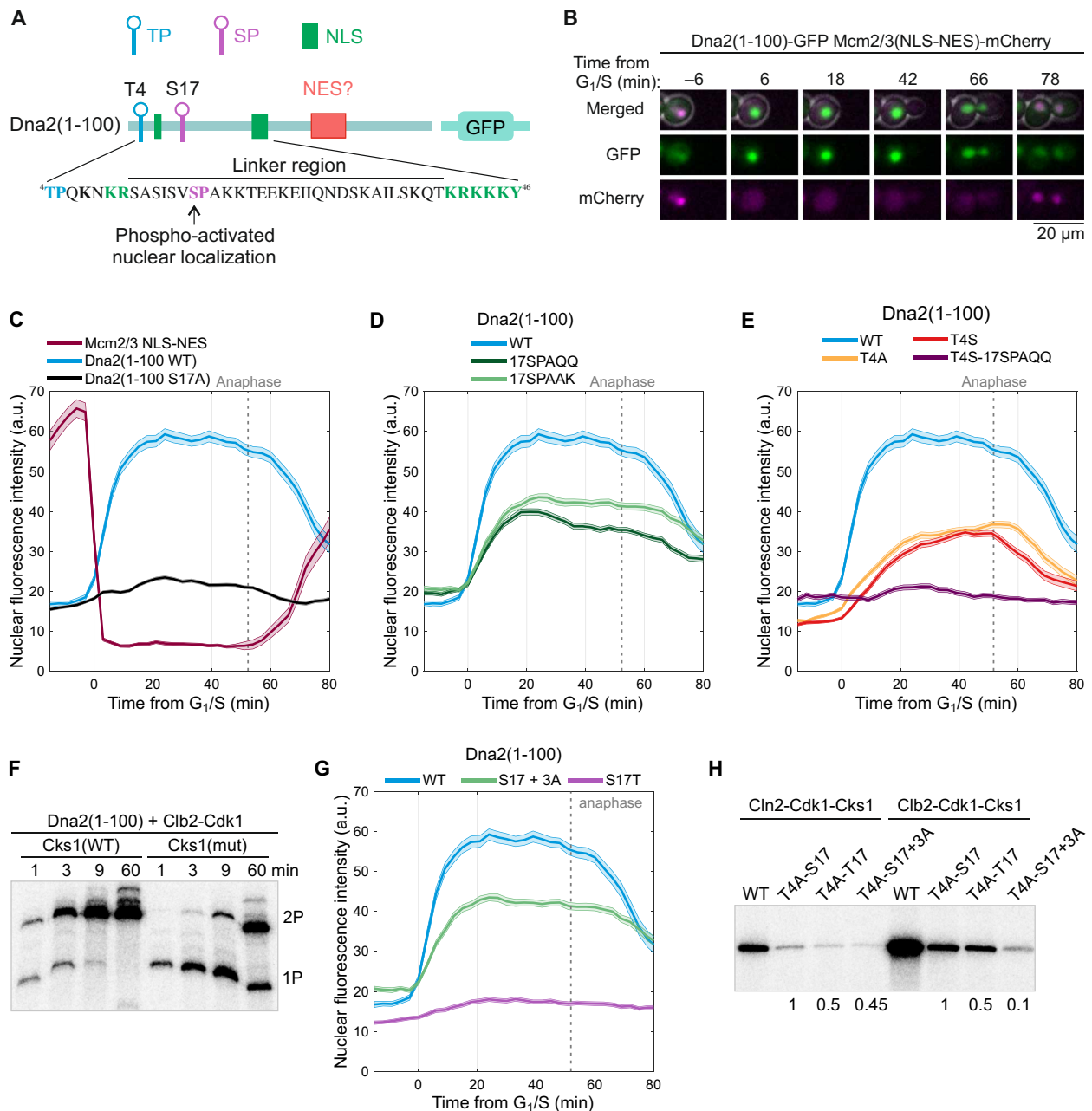


Fig. 5. Cdk1-regulated nuclear import of the Dna2 module. (A) Scheme showing the Cdk1 phosphorylation sites and localization motifs in the intrinsically disordered N terminus of Dna2, positions 1 to 100. (B) Microscopy images showing the localization of Dna2(1-100)-GFP and Mcm2/3(NLS-NES)-mCherry during the cell cycle. Imaging was done with 3-min interval; a selection of time points is shown. (C to E) Mean nuclear fluorescence levels of the indicated proteins during the cell cycle in a population of cells synchronized at the point of 50% nuclear export of Mcm2/3 NLS-NES sensor (denoted as time of G₁/S). The plot shows means ± SEM. (F) ³²P autoradiographs of Phos-tag SDS-PAGE gels showing the Cks1-dependence of the multisite phosphorylation of Dna2(1-100) by Clb2-Cdk1. (G) Effect of S17T mutation on the nuclear import of Dna2(1-100)-GFP. Plots show means ± SEM. (H) In vitro phosphorylation analysis of the indicated Dna2(1-100) mutants using Cln2- and Clb2-Cdk1. ³²P autoradiograph showing Dna2(1-100) phosphorylation under initial velocity conditions is shown.

was combined with the loss of Cks1 priming by T4S mutation, no nuclear accumulation of the module was observed during the cell cycle (Fig. 5E). This indicates that Cks1 docking is necessary to keep a substantial fraction of molecules phosphorylated at S17.

In a kinase assay followed by Phos-tag SDS-PAGE, rapid accumulation of a doubly phosphorylated form was observed, and this

process was severely suppressed by the Cks1 phospho-pocket mutation, confirming that Cks1 promotes multiphosphorylation of the module (Fig. 5F). We also performed Phos-tag Western blotting of synchronized yeast cultures to directly analyze the phosphorylation of Dna2(1-100)-GFP in the cell cycle. Dna2(1-100) was unphosphorylated in pheromone-induced G₁ arrest followed by extensive

phosphorylation at approximately 30 min after the cells were released from arrest (fig. S5B). Analysis of the multisite phosphorylation pattern of different Dna2(1-100) mutants confirmed that both T4 and S17 are phosphorylated in a cell cycle–dependent manner (fig. S5C).

As with the threonine versus serine effects observed in Psy4-based constructs, an S17T mutation in Dna2 led to a profound decrease in nuclear accumulation (Fig. 5G), and reduced phosphorylation of T17, but not S17, was also observed in Phos-tag Western blotting experiments in a T4A background (fig. S5C). The negative effect of S17T on entry was greater than that observed by mutating S17 to a minimal consensus site (S17 + 3A, mutation of 17SPAK to SPAA) (Fig. 5G). The S17T mutation caused a decrease in the phosphorylation rate by approximately two times with both Cln2-Cdk1 and Clb2-Cdk1 *in vitro* (Fig. 5H). Mutation of S17 to a minimal consensus site (S17 + 3A), however, led to a greater decrease in the phosphorylation rate (Fig. 5H). This suggests that factors other than CDK specificity are affected by Ser-to-Thr mutations *in vivo*. Again, as in Psy4, we hypothesize that this result could be due to the higher dephosphorylation rate of TP sites compared to SP sites (28). *In vitro* analysis of the phosphatase specificity of Dna2(1-100) confirmed that PP2A-Cdc55 preferentially dephosphorylates the S17T mutant, while the mitotic exit phosphatase Cdc14 preferentially targets S17 (fig. S5D).

Next, we tested the effect of added cyclin docking SLiMs in the Dna2-derived module. As the majority of its nuclear accumulation occurs around G₁/S, we hypothesized that this effect could be driven mainly by the G₁-specific Cln2-Cdk1 complex, which is abundant in the cytoplasm (47, 48). We introduced specific docking motifs for G₁-, S-, and M-Cdk1 to Dna2(1-100 17SPAQQ) (fig. S5E). The addition of a G₁-Cdk1–specific LP motif caused an approximately 10-min advance in nuclear entry and an increase in nuclear levels throughout the cell cycle (fig. S5F). Adding an S-Cdk1–specific NLxxxL motif did not affect the nuclear import dynamics of the module (fig. S5F), likely because the S phase cyclins are predominantly nuclear (37). The module containing a mitotic cyclin docking motif LxF showed similar nuclear entry at G₁/S as that of the WT but had a marked nuclear accumulation peak 40 to 60 min after G₁/S (fig. S5F). These results indicate that the G₁- and M-Cdk1 complexes play a major role in the phosphorylation of cytoplasmic targets. In contrast, the Psy4-based constructs were affected by the specificity of all four major cyclins, indicating that the nuclear export of CDK targets is affected by CDK activity in both compartments.

Programming the phosphorylation patterns to control protein oscillations in the nucleus

Our experiments have shown that the input activity of the core CDK oscillator can be processed into different output profiles of regulated dynamic processes. This can be achieved by combining the multisite phosphorylation code (26) and kinetics of the downstream event, which, in the current case, was nucleocytoplasmic shuttling. For a conclusive overview, we next demonstrate collected sets of nuclear oscillatory patterns of CDK outputs that were programmed into the studied modules using a small set of sequence elements that involved a combination of phosphorylation sites and cyclin docking sites. For a primary reference profile, one can consider the gradual decline of the T347A Psy4 sensor (Fig. 6A). Our study reveals that there are many ways to transform this gradual shape into various profiles. In all tested constructs, an abrupt change in the nuclear level of the Psy4 sensor occurred only around the time of G₁/S (0 min) and at mitotic entry (after 20 min). Addition of the RxL motif caused the

switch to be even more abrupt than that of the WT (Fig. 6A). A considerable delay that spanned S phase (approximately 20 min) could be introduced by mutating T320 and S364 and adding the M-CDK docking motif LxF. The constructs with intermediate timing between the G₁/S and M phase profiles were always exported in a stepwise manner, as shown by the construct with RxL cyclin docking sites in the T320A-S364A sensor (Fig. 6A).

Biphasic oscillatory profiles were also designed that contain one signaling output in S phase and another in mitosis (Fig. 6B). The level of S phase output could be slightly modulated, for example, by introducing the T320S mutation to the S364A background (Fig. 6B). Second, the gradual profile of T347A could be switched to a biphasic profile by the addition of a Clb5-specific NLxxxL docking site in the middle of the construct, while smooth nonswitch-like profiles were obtained when the docking site was introduced at the C terminus of the construct (Fig. 6C and fig. S6A). Given that the Clb5 docking motifs potentiate the phosphorylation of sites located N-terminally from the docking motif (41), this result suggests that the middle position helps to phosphorylate T320, imposing a stronger block to nuclear re-entry in S phase to create a biphasic profile. The C-terminal positioning of the docking motif also potentiates the phosphorylation of the NES-activating sites and therefore draws a profile with a faster exit than that of the gradual T347A reference profile.

For the Dna2-based sensors, the entry timing after G₁/S was sensitive to Cln2 specificity (an addition of an optimal LP docking site) (Fig. 6D and fig. S6B). Second, the efficiency of Cks1-mediated phosphorylation is known to be dependent on the distance between the primer and secondary sites, with the optimal distance window being estimated to fall between 12 and 16 amino acids (41). Increasing the distance between T4 and S17 by four amino acids considerably delayed entry (Fig. 6D and fig. S6B).

We found that different re-entry timings could also be programmed. The WT Psy4 module was imported approximately 5 min later than the Mcm2/3-based sensor (Fig. 6E). Mutation of sites S409A and S434A and single mutation of S364A led to earlier re-entry timing and resulted in higher nuclear levels in G₁ (Fig. 6E), presumably because the nuclear accumulation of these mutants is more dependent on dephosphorylation of the TP sites that are preferentially targeted by PP2A-Cdc55 (28). The T320S and T347S mutations also advanced nuclear import (Fig. 6E), likely because the phosphatase Cdc14 preferentially dephosphorylates SP sites (Fig. 3H) (44, 45).

Programming different stable nuclear plateau levels spanning from G₁/S to M/G₁

As observed in several cases for both the Psy4- and Dna2-based sensors, manipulating the phosphorylation sites and cyclin docking motifs often does not affect the timing of shuttling but instead leads to different steady states of nuclear levels that last for the whole span of S and M phases. For example, a lower constant nuclear accumulation could be programmed in the Dna2 sensor by mutating S17 to a minimal consensus site (17SPAQQ or 17SPAAK) (Fig. 7A and fig. S7A). The nuclear levels could also be lowered by increasing the distance between T4 and S17 (T4 + GGSG), resulting in a less efficient Cks1-mediated phosphorylation of S17 (Figs. 6D and 7A). The lowest nuclear level was observed with the S17T mutation (Fig. 7A). Furthermore, while the addition of a G₁-CDK–specific docking motif shifted the timing of nuclear entry, it also increased the constant plateau level (Fig. 6D). These results indicate that due to the

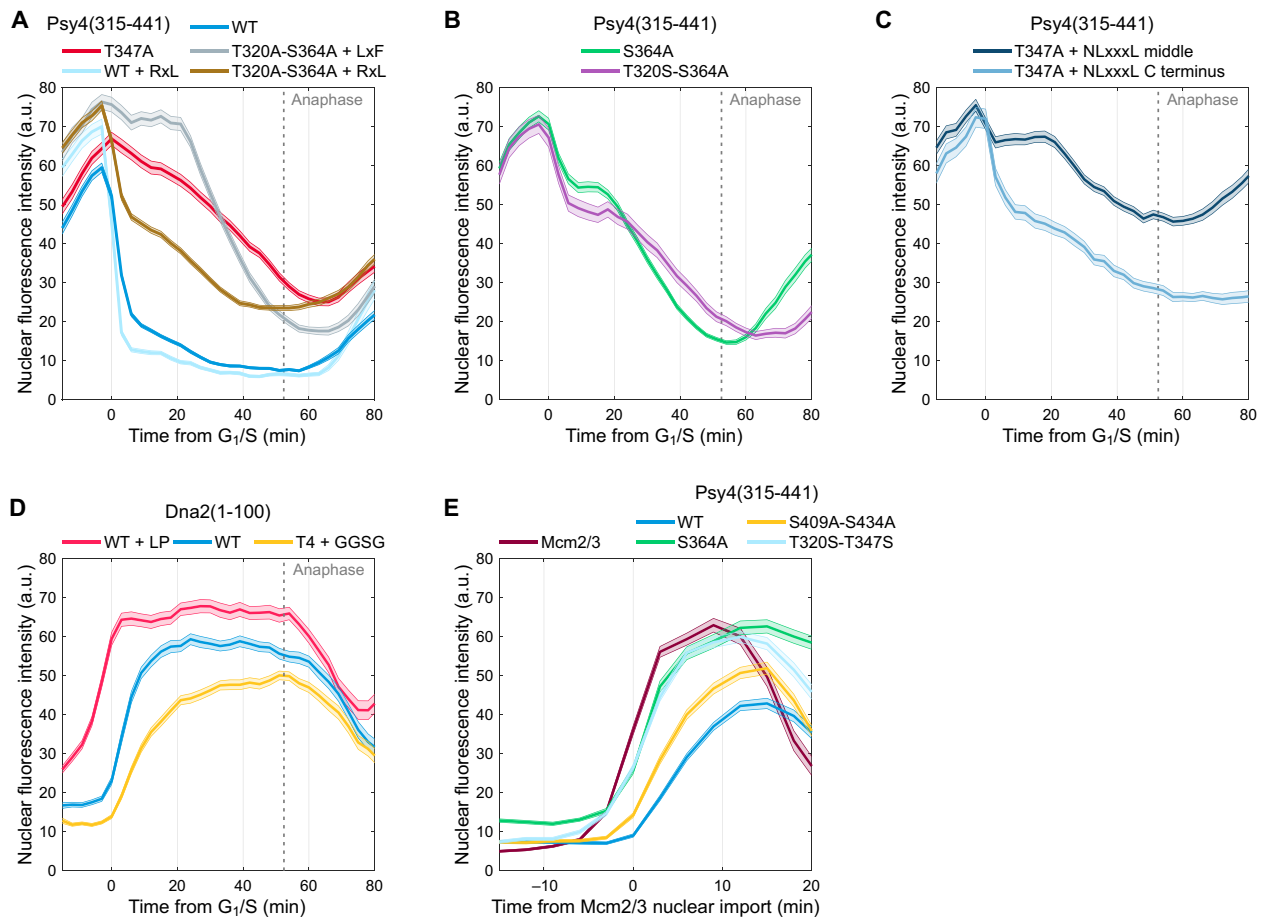


Fig. 6. Encoding of CDK-regulated localization modules with different output dynamics. (A to C) Plots showing means \pm SEM nuclear fluorescence intensities of the indicated Psy4(315-441)-GFP modules during the cell cycle. In (A) and (B), T347A, T320A S364A + RxL, T320A S364A + LxF, and S364A have been replotted from the data presented in Figs. 1 and 2 to illustrate different principles. (D) Plot displaying the timing of nuclear import of different Dna2(1-100)-GFP modules. Means \pm SEM of the nuclear fluorescence is shown. (E) Nuclear import of Psy4(315-441)-GFP in late mitosis was studied in time-lapse microscopy by synchronizing the cells at the nuclear import of 50% of the Mcm2/3-mCherry sensor. Plot shows means \pm SEM nuclear fluorescence levels.

different localization patterns of cyclins (37, 47, 49), CDK activity does not accumulate uniformly in the cytoplasm during the cell cycle. Apparently, the high cytoplasmic abundance of G₁ cyclin Cln2 could result in an early peak in cytoplasmic Cdk1 activity. This may be the cause of the nearly flat overall nuclear profile of the sensor, as the Dna2-based sensor is cytoplasmic in G₁, and NLS-activating phosphorylation as an entry trigger should also take place in the cytoplasm.

Similarly, in the Psy4- and Mcm2/3-based sensors, we demonstrated a wide-range ladder of controlled steady nuclear plateaus (Fig. 7B and fig. S7B). The lowest constant nuclear concentration from G₁/S to mitosis was achieved by adding a G₁-CDK docking motif to the WT Psy4 sensor, while the next step on the ladder could be achieved by further mutating the sites T320 and S364. The optimal LP motif efficiently targets G₁-Cdk1 activity to phosphorylate the Psy4 module, resulting in rapid nuclear exit at G₁/S. Then, a period with no further decrease in nuclear concentration occurs, presumably due to the degradation of Cln2 or because the modules are fully phosphorylated. As the T347A mutation prohibits full NLS inactivation, this mutant is expected to have higher nuclear abundance in the state in which all other sites are phosphorylated. Next, by replacing the native NES from Mcm3 with the weaker NES from Psy4,

an intermediate plateau was observed. As this replacement does not affect the phosphorylation sites adjacent to the Mcm3 NLS, phosphoregulation is likely unaffected, but a different nuclear-cytoplasmic ratio is achieved because of the relative strength of NLS and NES motifs. Using just a single weak NLS-inhibiting site and S/T swapping, two higher steps can be added to the ladder (Fig. 7B). While the module that carries S320 is partially translocated at G₁/S, the module with only T347 is not affected by progression to the S phase. Mutating the NES on the Mcm2/3-based sensor is among the other ways to fine-tune the higher levels of the nuclear plateau (Fig. 7B). Thus, tuning the NLS and NES activities by phosphorylation enables the creation of sensors with distinct nuclear-cytoplasmic ratios throughout the cell cycle.

DISCUSSION

Our study demonstrates that cyclins can create different oscillating protein localization shapes via CDK-driven phosphoregulation of NLS and NES signals. These oscillatory patterns depend on various parameters, including the kinetics of the downstream steps (nuclear entry and exit rates), phosphatase specificity, cyclin specificity in

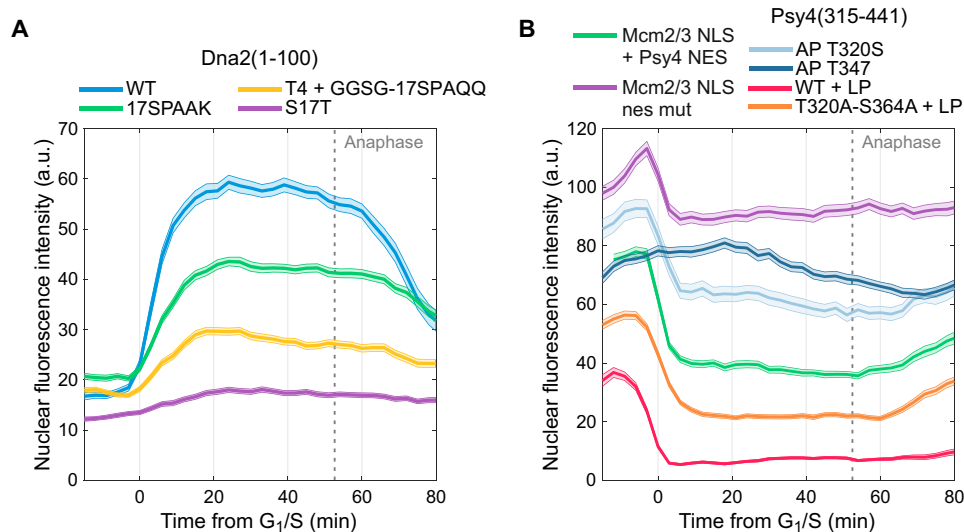


Fig. 7. Programming CDK signaling modules with different stable plateau levels. (A and B) Plots displaying means \pm SEM nuclear fluorescence intensities of Dna2-, Psy4-, and Mcm2/3-based localization modules measured in unperturbed cell cycles of single cells in time-lapse microscopy experiments. The schemes for the modules used in (B) are shown in fig. S7B. In (A), WT and S17T have been replotted from Fig. 5G for comparison with other constructs. In (B), different Psy4 constructs have been plotted together from earlier figures.

substrate docking, and Cks1-dependent phospho-docking connections. Our data suggest that the kinetics of downstream steps may be as important as the CDK/phosphatase activity thresholds in defining the order and temporal dynamics of CDK-driven events (fig. S1A). We also found that linking the NLS and NES phospho-regulation via Cks1-dependent docking may play an important part in establishing the nuclear import-export equilibria of CDK targets.

We observed that CDK-dependent fast export combined with the phosphorylation-induced block of re-entry can result in a very abrupt early nuclear exit switch. On the other hand, just a single alanine mutation (T347A) in the six-site network can change the profile from an ultrasensitive switch to a graded response. The gradual profile can be turned back to an abrupt switch by G_1 -CDK-specific docking. These observations are related to one of the important challenges in kinase signaling: how to process a graded input into an ultrasensitive all-or-none output (Fig. 8) (12). Furthermore, the T320A-S364A Psy4 sensor was not responsive to the accumulation of CDK activity until mitosis (Fig. 2A) (28). However, in mitosis, an ultrasensitive nuclear exit profile was formed, which was further enhanced by the addition of the M-CDK docking motif LxF (Figs. 2E and 8). Unexpectedly, when only the suboptimal CDK site S364 site was added back, the ultrasensitive exit profile was shifted by 30 min from the M phase to the G_1/S phase (Fig. 1D). Considering the 90-min span of the cell cycle, this reprogramming of the ultrasensitive output profiles with widely separated timing would likely be difficult to design by introducing only a minor change in the number of sites from six to four using a simple distributive multisite phosphorylation-based ultrasensitivity mechanism (12).

Comparing the rapid exit of the WT Psy4 sensor, the gradual exit of the T347A mutant, and the two-step exit with an S phase plateau of the AP T320-T347 Psy4 sensor shows that CDK targets with different multisite phosphorylation patterns can have very different response dynamics to the increasing CDK activity that drives the cell cycle progression (Fig. 8). This provides several interesting insights into cell cycle regulation. First, the presence of a plateau

indicates a rapid switch from low to high S phase CDK activity at G_1/S rather than a gradual increase in activity during the S phase. Second, the formation of a plateau suggests that an equilibrium in phosphorylation and dephosphorylation is reached in the AP T320-T347 mutant, in contrast to T347A mutant, where the equilibrium is not achieved in this time and the sensor exits gradually (Fig. 8). In AP T320-T347 sensor, the exit is dependent on phosphorylation of full consensus TP sites that are rapidly targeted both by Cdk1 and by phosphatase PP2A. In T347A, however, the gradual exit could be due to slow accumulation of phosphorylation at S364, S409, and S434, which are minimal consensus Cdk1 sites and suboptimal PP2A sites as they are serines. These differences indicate that the equilibrium is not reached rapidly for all CDK substrates.

To compare the mechanism of temporal resolution of CDK switches in the case of direct linear threshold-to-switch systems and the more complex equilibrium systems (NLS-NES), the concept of the “rate-limiting step” in CDK multisite phosphorylation systems must be considered. In our previous studies, we focused on the CDK multisite phosphorylation of targets with diphospho-degrons (26, 27). In these cases, the rate-limiting step was phosphorylation of a nonconsensus CDK site, a crucial part of the degron, which is the end output of the Cks1-driven multisite process. Without Cks1 and cyclin docking, these sites remain unphosphorylated even at the highest mitotic thresholds of CDK (26). Alternatively, in NLS-NES equilibrium-type Psy4-based sensors, there are two limiting steps and two outputs. High phosphatase activity limits the phosphorylation of NLS-regulating T320 and T347 (28), while phosphorylation of the export-promoting sites is limited by poor CDK specificity. Cks1-dependent docking links the NLS-inactivating sites and NES-activating sites. By changing the multisite phosphorylation patterns, shape and timing of the sensor localization profile could also be tuned (Fig. 8), which is a step further in complexity from the single degron. In addition, the priming and docking connection is specific for Cdk1 and not for other proline-directed kinases, including Fus3

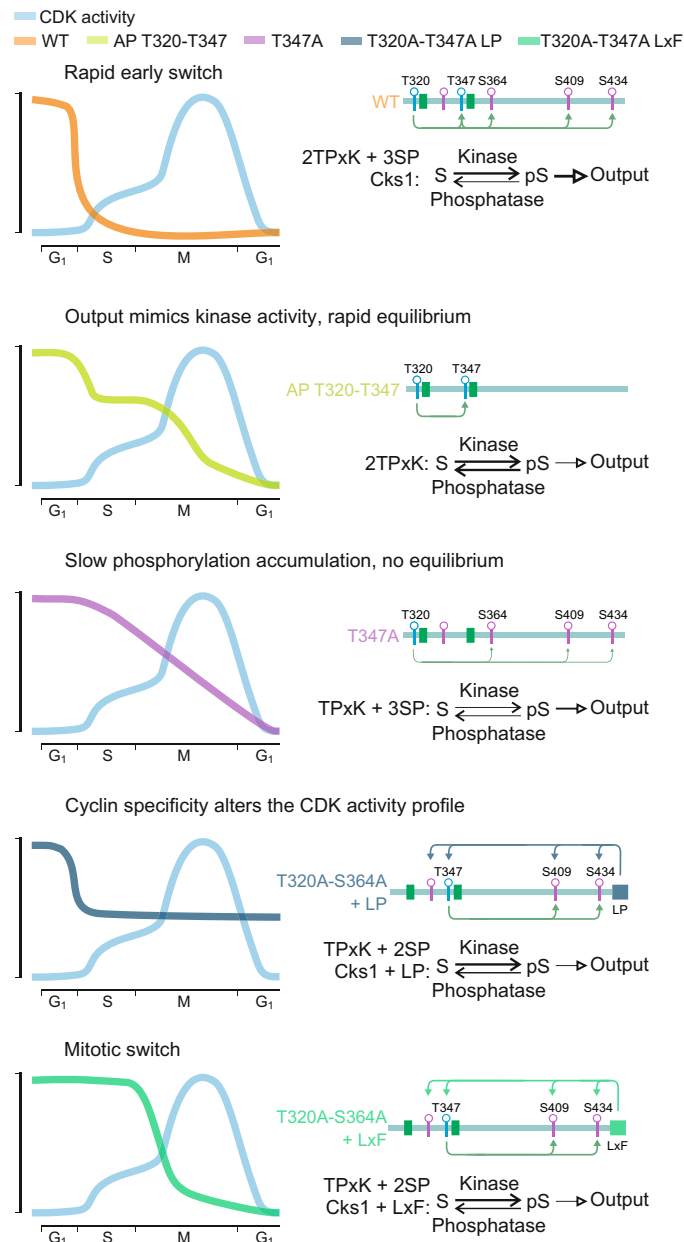


Fig. 8. Different response dynamics of the localization sensors to CDK activity during the cell cycle. Schemes that present the nuclear profiles obtained by different arrangements of the multisite phosphorylation network of a Psy4-type sensor. The light blue line shows an estimation of the CDK activity during the cell cycle. The colored arrows on the diagrams show enhancement of multisite phosphorylation by cyclin-specific docking sites (above the diagram) or by Cks1-dependent docking (below the diagram). The equilibriums show the net balance between phosphorylation and dephosphorylation, and the thick arrow on the right side of the equilibrium shows the overall export rate (exit and block of re-entry combined).

(fig. S4, A to C). Thus, the common feature of the two alternative systems is the Cks1-driven CDK filter that allows only CDK but not the other proline-directed kinases to trigger the switch. In case of degrons, different mutations influenced mainly the timing of degradation in the cell cycle and less the shape of the switch (26). This could be because degradation is an irreversible output, so an equilibrium is

not established. Together, these results illustrate the multitude of parameters that affect the dynamics of CDK substrate phosphorylation and highlight the importance of the output function in determining the phosphorylation threshold (fig. S1A).

Another important outcome of the study relates to our understanding of CDK thresholds and substrate sensitivity to CDK inhibition. According to the quantitative (or threshold) model of CDK function, more CDK activity is needed to drive mitosis than to trigger S phase, and this model is supported by the experimental evidence of different sensitivities of cell cycle transitions to Cdk1 inhibition (50, 51). The Cdk1-as1 strain can be arrested at G₂/M with 500 nM inhibitor and in both G₁ and G₂/M with a 5 μM dose (46, 50). According to the threshold model, the timing of cell cycle events is a product of the direct translation of accumulating CDK activity into the sequential timing of various phosphorylation switches. The faster the cyclin concentration rises, the earlier the switches should take place. However, paradoxically, overexpression, deletion of major cyclins, or placement of mitotic cyclin *CLB2* into S cyclin *CLB5* locus in yeast has only a minor effect on cell cycle dynamics (10, 52). These observations suggest the cell cycle progression is not considerably affected by premature accumulation of mitotic CDK activity. Similarly, the importance of dynamic dosing of CDK activity remains unclear in mammalian cells, as cyclin and Cdk knockouts revealed that the loss of several cyclins and Cdk is tolerated (53). Unexpectedly, we found that execution of the phosphorylation switch of a low-threshold G₁/S target, the Psy4-based sensor, is lost when Cdk1 activity is only slightly reduced, with a dose of 100 nM inhibitor (Fig. 4B). Thus, we cannot exclude the opposite possibility that the putative “high CDK threshold mitotic targets” that are responsible for low-dose (300 to 500 nM) inhibitor-induced G₂/M arrest (46, 50) may actually be phosphorylated at low CDK activity, as seen with Psy4-like inhibitor-sensitive low-threshold early G₁/S targets.

Intriguingly, the inherently weaker activity of Cdk1-as1 kinase results in a longer cell cycle, similar to yeast cells under poor nutrient conditions with slower cyclin accumulation (54–56). In rich media, as suggested by high tolerance to cyclin deletions, CDK activity accumulates excessively, perhaps to guarantee robustness. Under conditions with low net CDK activity, the phosphorylation of a minimal set of targets during a narrow low threshold window (potentially including those involved in mitotic events) could be sufficient to accomplish the cycle. Inhibitor-sensitive substrates such as Psy4, however, could be important for fine-tuning for better fitness in rich media with excess CDK activity.

The connection between phosphorylation specificity and CDK thresholds has yet another aspect, as the targets that must be 100% phosphorylated, for example, to prevent rereplication, should have higher phosphorylation specificity than those that can execute their downstream processes when partially phosphorylated (Fig. 4, D and E). We also cannot exclude an alternative possibility that the ability of cyclin specificity to temporally resolve different switches (26, 33) is not simply to time the onset of specific cell cycle processes but is instead needed to mitigate substrate competition. The cell contains hundreds of targets in which the *K_MS* are relatively low for particular cyclin-CDK complexes but high for the others (2, 34).

In conclusion, our results provide a broader view of the dynamics and specificity of CDK signaling, shedding light on how a single protein kinase can temporally coordinate such an intricate process as cell division. Our study also suggests that CDK-dependent phosphoregulation of NLS and NES motifs surrounded by different

multisite phosphorylation patterns can potentially be a flexible way to tune and dynamically control both entry-exit timing and the nuclear levels of CDK targets. Such a toolbox of multisite phosphorylation rules, described here and in our previous studies (26, 27), may prove to be useful in the next-generation synthetic circuit design for synthetic biology applications that aim to better control cellular signaling in a dynamic manner.

MATERIALS AND METHODS

Yeast strains and plasmids

S. cerevisiae strains were derived from W303 and are described in table S1. Gene deletions and tagging were performed using polymerase chain reaction and homologous recombination-based approach (57). Mcm2/3 NLS-NES (36) was cloned into pRS304 with P_{ADH1} and mCherry coding sequence. The plasmid was linearized with Pac I and integrated to P_{ADH1} locus. Psy4 and Dna2 nuclear localization modules were cloned into pRG203MX with P_{ACT1} and sfGFP (58). pRG203MX enables guaranteed single-copy integration of the vector (59). Before yeast transformation, the pRG203MX-based plasmids were linearized with Sgs I. The plasmids used for protein purification are described in table S2.

Time-lapse fluorescence microscopy

Before microscopy experiments, the cells were grown at 30°C in synthetic complete (SC) media supplemented with 2% glucose to OD₆₀₀ (optical density at 600 nm) of 0.2 to 0.6. The culture was pipetted on 0.8-mm cover glass and covered with a 1-mm-thick 1.5% agarose (NuSieve™ GTG™ Agarose, Lonza) SC/glucose pad. The sample was kept under the microscope for 1 hour before starting the experiment. The experiments were carried out using Zeiss Observer Z1 microscope with a 63×/1.4 numerical aperture oil immersion objective and AxioCam 506 mono camera (Zeiss). The sample was kept at 30°C with Tempcontrol 37-2 digital (PeCon). The cells were imaged for phase contrast, GFP, and mCherry with 3 × 3 binning every 3 min. The experiments were up to 8 hours long and up to 12 positions were followed using ZEN software (Zeiss), an automated stage, and Definite Focus. Filter Set 61 HE (Zeiss) in combination with Colibri 470 and Colibri 540 to 580 light-emitting diode (LED) modules with exposure times of 15 and 450 ms was used for imaging of sfGFP and mCherry, respectively. The Colibri LED modules were used at 25% power.

Image segmentation, cell tracking, and quantification of fluorescence signals were performed using MATLAB (The MathWorks Inc.) as described in (60). To analyze nuclear levels of the fluorescent proteins, the brighter region of the cell was segmented as the nucleus and the cytoplasm was considered as background signal, as the same amounts of the fluorescent proteins have very low signals when diluted into the cytoplasm. Also, as the cytoplasmic fluorescent protein signal overlaps with the nuclear signal, the average cytoplasmic signal is subtracted from the average nuclear signal to obtain the final nuclear fluorescence intensities shown on the plots. All plots with microscopy data contain data from at least two biological replicate experiments, and the number of cells analyzed from each construct is presented in table S1. The time when 25% of cells [based on Psy4(315-441 WT)-GFP strain] reaches anaphase is marked on the plots (54 min from G₁/S). This was measured from the nuclear entry of Mcm2/3-mCherry, which we have determined previously to take place 11.5 min after the onset of spindle elongation or anaphase

(18). No cells or replicate experiments were excluded from the analysis. The data are plotted as the average nuclear fluorescence intensities of a population of cells from multiple experiments. The error bars are ±SEM. No sample size precalculations were made. Fifty cells were considered to be sufficient for the analysis, because replicate experiments with such sample size showed very little variation.

Western blotting

Dna2(1-100)-sfGFP and Psy4(315-441)-sfGFP were tagged with 6 copies of human influenza hemagglutinin epitope tag (6HA) as described in (57). The yeast cultures were grown at 30°C in yeast extract, peptone, and dextrose (YPD) medium to OD₆₀₀ of 0.3, followed by addition of α -factor (1 μ g/ml) and incubation for 2.5 hours to arrest cells in G₁ phase. Then, the cells were washed thoroughly to remove α -factor and were resuspended in fresh YPD medium and grown at 30°C. Cells from 5 ml of the culture were collected and flash-frozen in liquid nitrogen every 10 min.

Cells were lysed by bead beating in lysis buffer containing urea. The proteins were separated using Phos-tag SDS-PAGE with 8% acrylamide, 50 μ M Phos-tag, and 100 μ M MnCl₂ as described in (61). The electrophoresis was carried out at 15 mA for 1.5 hours. Before transfer, the gels were soaked in tris-buffered saline with Tween 20 buffer containing 10 mM EDTA for 30 min. The transfer to nitrocellulose membrane was performed using the standard semidry transfer with Pierce G2 Fast Blotter (Thermo Fisher Scientific). Purified anti-HA.11 epitope tag antibody (1:500) (clone 16B12, BioLegend, catalog no. 901501, RRID:AB_2565006) and horseradish peroxidase-conjugated anti-mouse antibody (1:7500) from LabAs, Estonia were used to detect the 6HA-tagged proteins. All Western blotting experiments were done in at least two biological replicates.

Protein purification

Dna2(1-100)-sfGFP, Psy4(315-441)-sfGFP, Sic1, and Cdc14 were cloned to pET28a and were expressed in *Escherichia coli* BL21RP cells as fusion proteins with N-terminal 6xHis tag. Sic1 was expressed at 37°C using 1 mM isopropyl- β -D-thiogalactopyranoside (IPTG), while Dna2 and Psy4 constructs were expressed at 30°C using 0.5 mM IPTG. The proteins were purified using immobilized cobalt affinity chromatography and imidazole for elution. The expression of 6xHis-Cdc14 was induced with 0.125 mM IPTG at 23°C, followed by purification using nickel affinity chromatography.

Clb2-Cdk1 and Clb5-Cdk1 complexes were purified from yeast extract of the respective tagged cyclin overexpression culture using tandem affinity purification method as described previously (6, 62). For purification of Cln2-Cdk1, Cln2 was N-terminally tagged with 3HA, overexpressed from P_{GAL1} promoter, and purified using immunoaffinity chromatography as described previously (63). Cks1 was purified from *E. coli* BL21RP extracts as described in (64).

PP2A-Cdc55 complex was purified from yeast cells containing 3HA-tagged Cdc55 (65). The yeast culture was grown in YPD to OD₆₀₀ of 1.4, and the cells were collected, snap-frozen, and lysed using Mixer Mill MM 400. The lysate was cleared by centrifugation, and the supernatant was incubated with anti-HA agarose beads for 3 hours. The beads were washed thoroughly, and PP2A-Cdc55 was eluted with buffer containing HA dipeptide.

In vitro phosphorylation assays

The general composition of the phosphorylation experiments was as follows: 50 mM HEPES-KOH (pH 7.4), 150 mM NaCl, 5 mM MgCl₂,

20 mM imidazole, 2% glycerol, bovine serum albumin (BSA) (0.2 mg/ml), 500 nM Cks1, and 500 μ M adenosine triphosphate (ATP) [(with added [γ - 32 P]-ATP (Hartmann Analytic)]. The substrate protein concentration was 1 μ M [in the linear (S) versus initial velocity range, several-fold below the estimated K_M value], and cyclin-Cdk1 complex concentration was 0.2 nM. The reactions were carried out at room temperature and were stopped at the indicated time points by addition of SDS-PAGE sample buffer. For analysis of multisite phosphorylation, the proteins were separated using Phos-tag SDS-PAGE (8% acrylamide and 50 μ M Phos-tag) as described in (61).

For the dephosphorylation assays, the Dna2- and Psy4-based purified substrate proteins were phosphorylated with Clb5-Cdk1 at room temperature for 20 (Psy4) or 60 (Dna2) min in the following buffer: 20 mM tris-HCl (pH 7.4), 50 mM Hepes-KOH (pH 7.4), 210 mM NaCl, 5 mM MgCl₂, 80 mM imidazole, 2% glycerol, BSA (0.2 mg/ml), and 500 μ M ATP [(with added [γ - 32 P]-ATP (Hartmann Analytic)]. Then, an aliquot of the reaction was pipetted to SDS-PAGE sample buffer to measure the phosphorylated protein 32 P signal, and a mixture containing Sic1 and either Cdc14 or PP2A-Cdc55 phosphatase was added to the rest of the phosphorylation reaction. Sic1 was added to inhibit further phosphorylation of the substrate proteins by Clb5-Cdk1. At 5, 20, and 60 min, an aliquot of the reaction was pipetted to SDS-PAGE sample buffer to stop the dephosphorylation reaction. The samples were run on SDS-PAGE, the gels were dried, and 32 P signals were detected using an Amersham Typhoon 5 Biomolecular Imager (GE Healthcare Life Sciences) and were quantified using ImageQuant TL (Amersham Biosciences). All in vitro phosphorylation assays were performed in at least duplicates.

SUPPLEMENTARY MATERIALS

Supplementary material for this article is available at <https://science.org/doi/10.1126/sciadv.abp8992>

[View/request a protocol for this paper from Bio-protocol.](#)

REFERENCES AND NOTES

- Bloom, F. R. Cross, Multiple levels of cyclin specificity in cell-cycle control. *Nat. Rev. Mol. Cell Biol.* **8**, 149–160 (2007).
- M. Köivomägi, E. Valk, R. Venta, A. Iofik, M. Lepiku, D. O. Morgan, M. Loog, Dynamics of Cdk1 substrate specificity during the cell cycle. *Mol. Cell* **42**, 610–623 (2011).
- B. R. Topacio, E. Zatulovskiy, S. Cristea, S. Xie, C. S. Tambo, S. M. Rubin, J. Sage, M. Köivomägi, J. M. Skotheim, Cyclin D-Cdk4,6 drives cell-cycle progression via the Retinoblastoma Protein's C-terminal helix. *Mol. Cell* **74**, 758–770.e4 (2019).
- M. Köivomägi, M. P. Swaffer, J. J. Turner, G. Marinov, J. M. Skotheim, G1 cyclin-Cdk promotes cell cycle entry through localized phosphorylation of RNA polymerase II. *Science* **374**, 347–351 (2021).
- D. O. Morgan, *The Cell Cycle: Principles of Control* (New Science Press, 2007).
- J. A. Ubersax, E. L. Woodbury, P. N. Quang, M. Paraz, J. D. Blethrow, K. Shah, K. M. Shokat, D. O. Morgan, Targets of the cyclin-dependent kinase Cdk1. *Nature* **425**, 859–864 (2003).
- J. M. Enserink, R. D. Kolodner, An overview of Cdk1-controlled targets and processes. *Cell Div.* **5**, 11 (2010).
- S. Kosugi, M. Hasebe, M. Tomita, H. Yanagawa, Systematic identification of cell cycle-dependent yeast nucleocytoplasmic shuttling proteins by prediction of composite motifs. *Proc. Natl. Acad. Sci. U.S.A.* **106**, 10171–10176 (2009).
- J. D. Nardozi, K. Lott, G. Cingolani, Phosphorylation meets nuclear import: A review. *Cell Commun. Signal.* **8**, 32 (2010).
- D. Pirincci Ercan, F. Chrétien, P. Chakravarty, H. R. Flynn, A. P. Snijders, F. Uhlmann, Budding yeast relies on G1 cyclin specificity to couple cell cycle progression with morphogenetic development. *Sci. Adv.* **7**, eabg0007 (2021).
- J. E. Ferrell, Tripping the switch fantastic: How a protein kinase cascade can convert graded inputs into switch-like outputs. *Trends Biochem. Sci.* **21**, 460–466 (1996).
- J. E. Ferrell, S. H. Ha, S. H. Ha, Ultrasensitivity part II: Multisite phosphorylation, stoichiometric inhibitors, and positive feedback. *Trends Biochem. Sci.* **39**, 556–569 (2014).
- M. Thomson, J. Gunawardena, Unlimited multistability in multisite phosphorylation systems. *Nature* **460**, 274–277 (2009).
- J. B. Asfaha, M. Örd, C. R. Carlson, I. Faustova, M. Loog, D. O. Morgan, Multisite phosphorylation by Cdk1 initiates delayed negative feedback to control mitotic transcription. *Curr. Biol.* **32**, 256–263.e4 (2022).
- J. R. Pomeroy, E. D. Sontag, J. E. Ferrell Jr., Building a cell cycle oscillator: Hysteresis and bistability in the activation of Cdc2. *Nat. Cell Biol.* **5**, 346–351 (2003).
- L. Ou, M. B. Waddell, R. W. Kriwacki, Mechanism of cell cycle entry mediated by the intrinsically disordered protein, p27Kip1. *ACS Chem. Biol.* **7**, 678–682 (2012).
- R. Venta, E. Valk, M. Örd, O. Košik, K. Pääbo, A. Maljavin, R. Kivi, I. Faustova, N. Shtaida, M. Lepiku, K. Möll, A. Doncic, M. Köivomägi, M. Loog, A processive phosphorylation circuit with multiple kinase inputs and mutually diversional routes controls G1/S decision. *Nat. Commun.* **11**, 1836 (2020).
- M. Örd, R. Venta, K. Möll, E. Valk, M. Loog, Cyclin-specific docking mechanisms reveal the complexity of M-CDK function in the cell cycle. *Mol. Cell* **75**, 76–89.e3 (2019).
- J. Gerardin, N. R. Reddy, W. A. Lim, The design principles of biochemical timers: Circuits that discriminate between transient and sustained stimulation. *Cell Syst.* **9**, 297–308.e2 (2019).
- J. R. Burke, G. L. Hura, S. M. Rubin, Structures of inactive retinoblastoma protein reveal multiple mechanisms for cell cycle control. *Genes Dev.* **26**, 1156–1166 (2012).
- R. M. Gordley, R. E. Williams, C. J. Bashor, J. E. Toettcher, S. Yan, W. A. Lim, Engineering dynamical control of cell fate switching using synthetic phospho-regulons. *Proc. Natl. Acad. Sci.* **113**, 13528–13533 (2016).
- S. Liokatis, A. Stützer, S. Elsässer, F. Theillet, R. Klingberg, B. van Rossum, D. Schwarzer, C. Allis, W. Fischle, P. Selenko, Phosphorylation of histone H3 Ser10 establishes a hierarchy for subsequent intramolecular modification events. *Nat. Struct. Mol. Biol.* **19**, 819–823 (2012).
- A. Mylona, F.-X. Theillet, C. Foster, T. M. Cheng, F. Miralles, P. A. Bates, P. Selenko, R. Treisman, Opposing effects of Elk-1 multisite phosphorylation shape its response to ERK activation. *Science* **354**, 233–237 (2016).
- N. A. Lyons, B. R. Fonslow, J. K. Diedrich, J. R. Yates III, D. O. Morgan, D. O. Morgan, Sequential primed kinases create a damage-responsive phosphodegron on Eco1. *Nat. Struct. Mol. Biol.* **20**, 194–201 (2013).
- M. Köivomägi, E. Valk, R. Venta, A. Iofik, M. Lepiku, E. R. M. Balog, S. M. Rubin, D. O. Morgan, M. Loog, Cascades of multisite phosphorylation control Sic1 destruction at the onset of S phase. *Nature* **480**, 128–131 (2011).
- M. Örd, K. Möll, A. Agerova, R. Kivi, I. Faustova, R. Venta, E. Valk, M. Loog, Multisite phosphorylation code of CDK. *Nat. Struct. Mol. Biol.* **26**, 649–658 (2019).
- I. Faustova, L. Bulatovic, F. Matiyevskaya, E. Valk, M. Örd, M. Loog, A new linear cyclin docking motif that mediates exclusively S-phase CDK-specific signaling. *EMBO J.* **40**, e105839 (2021).
- M. Godfrey, S. A. Touati, M. Kataria, A. Jones, A. P. Snijders, F. Uhlmann, PP2A^{Cdc55} phosphatase imposes ordered cell-cycle phosphorylation by opposing threonine phosphorylation. *Mol. Cell* **65**, 393–402.e3 (2017).
- B. A. Schulman, D. L. Lindstrom, E. D. Harlow, Substrate recruitment to cyclin-dependent kinase 2 by a multipurpose docking site on cyclin A. *Proc. Natl. Acad. Sci. U.S.A.* **95**, 10453–10458 (1998).
- J. A. Wohlschlegel, B. T. Dwyer, D. Y. Takeda, A. Dutta, Mutational analysis of the Cy motif from p21 reveals sequence degeneracy and specificity for different cyclin-dependent kinases. *Mol. Cell Biol.* **21**, 4868–4874 (2001).
- S. Bhaduri, P. M. Pryciak, Cyclin-specific docking motifs promote phosphorylation of yeast signaling proteins by G1/S Cdk complexes. *Curr. Biol.* **21**, 1615–1623 (2011).
- S. Bandyopadhyay, S. Bhaduri, M. Örd, N. E. Davey, M. Loog, P. M. Pryciak, Comprehensive analysis of G1 cyclin docking motif sequences that control CDK regulatory potency in vivo. *Curr. Biol.* **30**, 4454–4466.e5 (2020).
- M. Örd, K. K. Puss, R. Kivi, K. Möll, T. Ojala, I. Borovko, I. Faustova, R. Venta, E. Valk, M. Köivomägi, M. Loog, Proline-rich motifs control G2-CDK target phosphorylation and priming an anchoring protein for polo kinase localization. *Cell Rep.* **31**, 107757 (2020).
- M. Loog, D. O. Morgan, Cyclin specificity in the phosphorylation of cyclin-dependent kinase substrates. *Nature* **434**, 104–108 (2005).
- B. O'Neill, S. J. Szjyka, E. T. Lis, A. O. Bailey, J. R. Yates, O. M. Aparicio, F. E. Romesberg, Pph3–Psy2 is a phosphatase complex required for Rad53 dephosphorylation and replication fork restart during recovery from DNA damage. *Proc. Natl. Acad. Sci.* **104**, 9290–9295 (2007).
- M. E. Liku, V. Q. Nguyen, A. W. Rosales, K. Irie, J. J. Li, CDK phosphorylation of a novel NLS-NES module distributed between two subunits of the Mcm2-7 complex prevents chromosomal rereplication. *Mol. Biol. Cell* **16**, 5026–5039 (2005).
- F. R. Cross, M. Yuste-Rojas, S. Gray, M. D. Jacobson, Specialization and targeting of B-type cyclins. *Mol. Cell* **4**, 11–19 (1999).
- F. Hu, O. M. Aparicio, Swe1 regulation and transcriptional control restrict the activity of mitotic cyclins toward replication proteins in *Saccharomyces cerevisiae*. *Proc. Natl. Acad. Sci. U.S.A.* **102**, 8910–8915 (2005).
- M. J. DeVit, M. Johnston, The nuclear exportin Msn5 is required for nuclear export of the Mig1 glucose repressor of *Saccharomyces cerevisiae*. *Curr. Biol.* **9**, 1231–1241 (1999).

40. D. A. McGrath, E. R. M. Balog, M. Köivomägi, R. Lucena, M. V. Mai, A. Hirschi, D. R. Kellogg, M. Loog, S. M. Rubin, Cks confers specificity to phosphorylation-dependent CDK signaling pathways. *Nat. Struct. Mol. Biol.* **20**, 1407–1414 (2013).
41. M. Köivomägi, M. Örd, A. Iofik, E. Valk, R. Venta, I. Faustova, R. Kivi, E. R. M. Balog, S. M. Rubin, M. Loog, Multisite phosphorylation networks as signal processors for Cdk1. *Nat. Struct. Mol. Biol.* **20**, 1415–1424 (2013).
42. K. Suzuki, K. Sako, K. Akiyama, M. Isoda, C. Senoo, N. Nakajo, N. Sagata, Identification of non-Ser/Thr-Pro consensus motifs for Cdk1 and their roles in mitotic regulation of C2H2 zinc finger proteins and Ect2. *Sci. Rep.* **5**, 7929 (2015).
43. M. J. Cundell, L. H. Hutter, R. Nunes Bastos, E. Poser, J. Holder, S. Mohammed, B. Novak, F. A. Barr, A PP2A-B55 recognition signal controls substrate dephosphorylation kinetics during mitotic exit. *J. Cell Biol.* **214**, 539–554 (2016).
44. S. C. Bremmer, H. Hall, J. S. Martinez, C. L. Eissler, T. H. Hinrichsen, S. Rossie, L. L. Parker, M. C. Hall, H. Charbonneau, Cdc14 phosphatases preferentially dephosphorylate a subset of cyclin-dependent kinase (Cdk) sites containing phosphoserine. *J. Biol. Chem.* **287**, 1662–1669 (2012).
45. S. A. Touati, L. Hofbauer, A. W. Jones, A. P. Snijders, G. Kelly, F. Uhlmann, Cdc14 and PP2A phosphatases cooperate to shape phosphoproteome dynamics during mitotic exit. *Cell Rep.* **29**, 2105–2119.e4 (2019).
46. A. C. Bishop, J. A. Ubersax, D. T. Pötsch, D. P. Matheos, N. S. Gray, J. Blethrow, E. Shimizu, J. Z. Tsien, P. G. Schultz, M. D. Rose, J. L. Wood, D. O. Morgan, K. M. Shokat, A chemical switch for inhibitor-sensitive alleles of any protein kinase. *Nature* **407**, 395–401 (2000).
47. N. P. Edgington, B. Futcher, Relationship between the function and the location of G1 cyclins in *S. cerevisiae*. *J. Cell Sci.* **114**, 4599–4611 (2001).
48. M. E. Miller, F. R. Cross, Distinct subcellular localization patterns contribute to functional specificity of the Cln2 and Cln3 cyclins of *Saccharomyces cerevisiae*. *Mol. Cell. Biol.* **20**, 542–555 (2000).
49. E. Bailly, S. Cabantous, D. Sondaz, A. Bernadac, M.-N. Simon, Differential cellular localization among mitotic cyclins from *Saccharomyces cerevisiae*: A new role for the axial budding protein Bud3 in targeting Clb2 to the mother-bud neck. *J. Cell Sci.* **116**, 4119–4130 (2003).
50. D. Coudreuse, P. Nurse, Driving the cell cycle with a minimal CDK control network. *Nature* **468**, 1074–1079 (2010).
51. D. L. Fisher, P. Nurse, A single fission yeast mitotic cyclin B p34cdc2 kinase promotes both S-phase and mitosis in the absence of G1 cyclins. *EMBO J.* **15**, 850–860 (1996).
52. C. Oikonomou, F. R. Cross, Rising cyclin-CDK levels order cell cycle events. *PLOS ONE* **6**, e20788 (2011).
53. A. Satyanarayana, P. Kaldis, Mammalian cell-cycle regulation: Several Cdks, numerous cyclins and diverse compensatory mechanisms. *Oncogene* **28**, 2925–2939 (2009).
54. B. L. Schneider, J. Zhang, J. Markwardt, G. Tokiwa, T. Volpe, S. Honey, B. Futcher, Growth rate and cell size modulate the synthesis of, and requirement for, G1 -phase cyclins at start. *Mol. Cell. Biol.* **24**, 10802–10813 (2004).
55. A. Jasani, T. Huynh, D. R. Kellogg, Growth-dependent activation of protein kinases suggests a mechanism for measuring cell growth. *Genetics* **215**, 729–746 (2020).
56. R. M. Leitao, D. R. Kellogg, The duration of mitosis and daughter cell size are modulated by nutrients in budding yeast. *J. Cell Biol.* **216**, 3463–3470 (2017).
57. C. Janke, M. M. Magiera, N. Rathfelder, C. Taxis, S. Reber, H. Maekawa, A. Moreno-Borchart, G. Doenges, E. Schwob, E. Schiebel, M. Knop, A versatile toolbox for PCR-based tagging of yeast genes: New fluorescent proteins, more markers and promoter substitution cassettes. *Yeast* **21**, 947–962 (2004).
58. J. D. Pédelacq, S. Cabantous, T. Tran, T. C. Terwilliger, G. S. Waldo, Engineering and characterization of a superfolder green fluorescent protein. *Nat. Biotechnol.* **24**, 79–88 (2006).
59. R. Gnügge, T. Liphardt, F. Rudolf, A shuttle vector series for precise genetic engineering of *Saccharomyces cerevisiae*. *Yeast* **33**, 83–98 (2016).
60. A. Doncic, U. Eser, O. Atay, J. M. Skotheim, An algorithm to automate yeast segmentation and tracking. *PLOS ONE* **8**, e57970 (2013).
61. M. Örd, M. Loog, in *Methods in Molecular Biology* (Humana Press Inc., 2020), vol. 2141, pp. 779–792.
62. O. Puig, F. Caspary, G. Rigaut, B. Rutz, E. Bouveret, E. Bragado-Nilsson, M. Wilm, B. Séraphin, The Tandem Affinity Purification (TAP) Method: A general procedure of protein complex purification. *Methods* **24**, 218–229 (2001).
63. D. McCusker, C. Denison, S. Anderson, T. A. Egelhofer, J. R. Yates III, S. P. Gygi, D. R. Kellogg, Cdk1 coordinates cell-surface growth with the cell cycle. *Nat. Cell Biol.* **9**, 506–515 (2007).
64. G. J. Reynard, W. Reynolds, R. Verma, R. J. Deshaies, Cks1 is required for G(1) cyclin-cyclin-dependent kinase activity in budding yeast. *Mol. Cell. Biol.* **20**, 5858–5864 (2000).
65. S. D. Anastasia, D. L. Nguyen, V. Thai, M. Meloy, T. MacDonough, D. R. Kellogg, A link between mitotic entry and membrane growth suggests a novel model for cell size control. *J. Cell Biol.* **197**, 89–104 (2012).

Acknowledgments: We thank E. Valk for support and D. Morgan, J. Skotheim, P. Pryciak, and D. Kellogg for valuable comments on the manuscript. **Funding:** This work was supported by ERC Consolidator Grant 649124 (to M.Lo.), Centre of Excellence for Molecular Cell Technologies TK143 (to M.Lo.), and Estonian Research Council grant PRG550 (to M.Lo.). **Author contributions:** Conceptualization: I.F., M.Ö., and M.Lo. Methodology: I.F., M.Ö., M.Lö., and M.Lo. Software: M.Ö. Investigation: I.F., M.Ö., V.K., D.F., I.B., K.P., M.Lö., and M.Lo. Resources: I.F., M.Ö., I.B., D.F., V.K., M.Lö., D.M., and M.Lo. Writing: I.F., M.Ö., and M.Lo. Visualization: I.F., M.Ö., and M.Lo. Supervision: I.F., M.Ö., and M.Lo. Funding acquisition: M.Lo. **Competing interests:** The authors declare that they have no competing interests. **Data and materials availability:** All data needed to evaluate the conclusions in the paper are present in the paper and/or the Supplementary Materials. The MATLAB code for analysis of time-lapse fluorescence microscopy experiments is available at <https://doi.org/10.5281/zenodo.6655336>.

Submitted 7 March 2022
Accepted 28 June 2022
Published 17 August 2022
10.1126/sciadv.abp8992